2018 Spring

“Advanced Physical Metallurgy”

- Bulk Metallic Glasses -

05.16.2018

Eun Soo Park

Office: 33-313
Telephone: 880-7221
Email: espark@snu.ac.kr
Office hours: by appointment

5.7. Annealing of Bulk Metallic Glasses: SR → SCLR (& PS) → Crystallization

5.7.1 Structural Relaxation

RELAXATION BEHAVIOR

Structural relaxation = stabilization

On annealing, the as-synthesized glass slowly transforms toward an "ideal" glass of lower energy through structural relaxation. = annihilation of "defects" or free volume, or recombination of the defects of opposing character, or by changes in both topological and compositional SRO

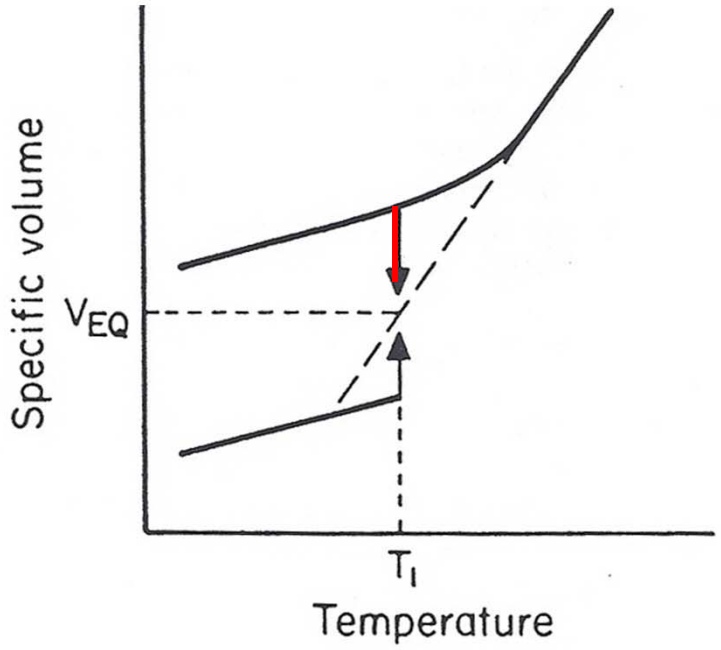

Fig. 9a. Relaxation from initial volumes above and below the equilibrium volume (schematic)

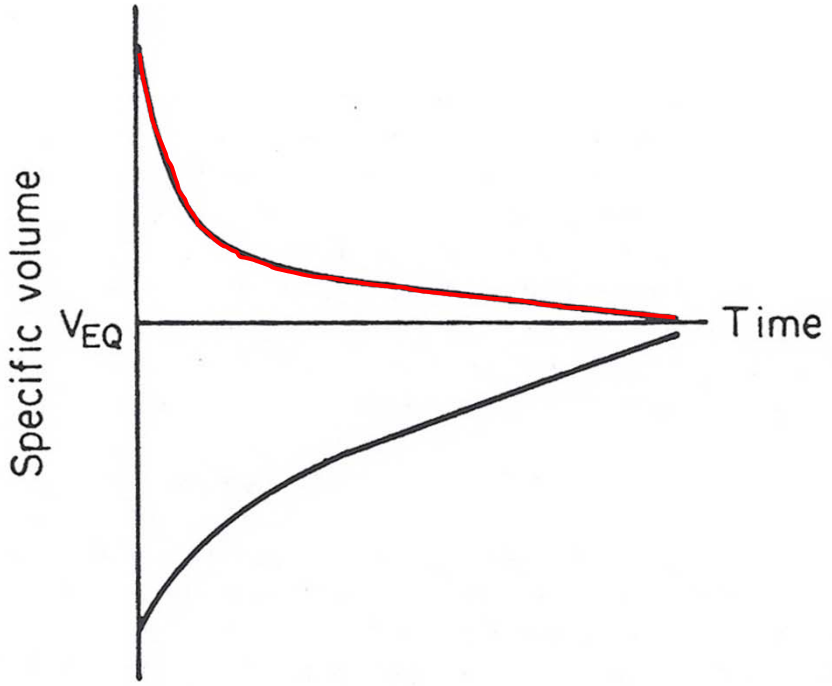

Fig. 9b. Variation of volume with time for initial volumes above and below the equilibrium volume (schematic)

Temperature dependence of relaxation time
: α relaxation (VFT) & β relaxation (Arrhenius)

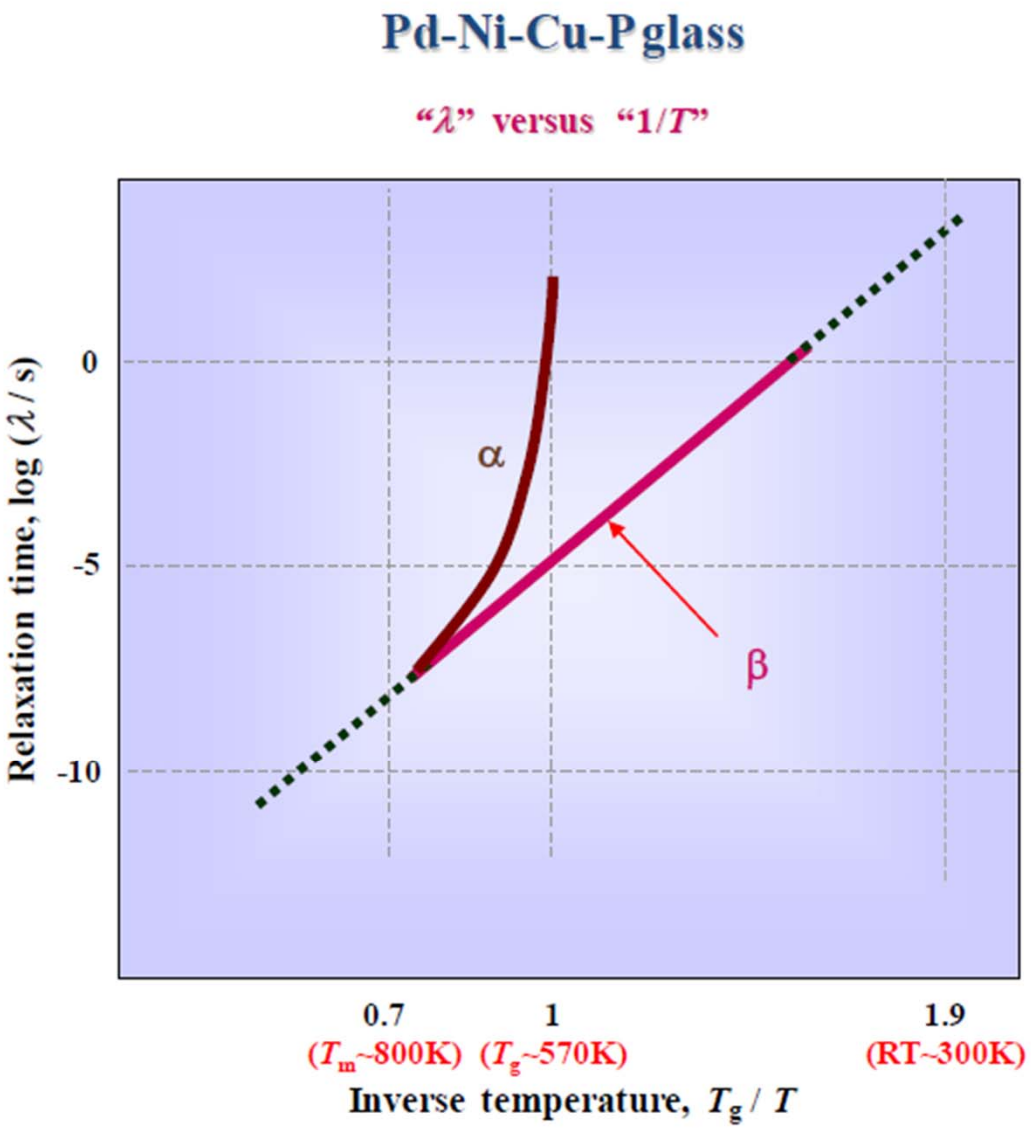

α VFT

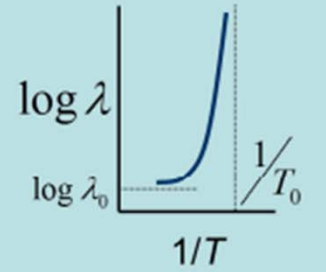

$$\lambda_\alpha = \lambda_{\alpha 0} \exp\left(\frac{Q_\alpha}{T - T_0}\right)$$

Arrhenius β

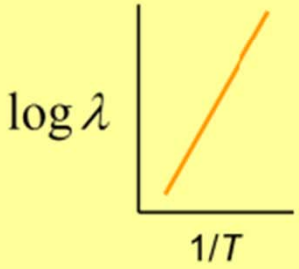

$$\lambda_\beta = \lambda_{\beta,0} \exp\left(\frac{Q_\beta}{kT}\right)$$

Dynamic mechanical relaxations in typical glasses

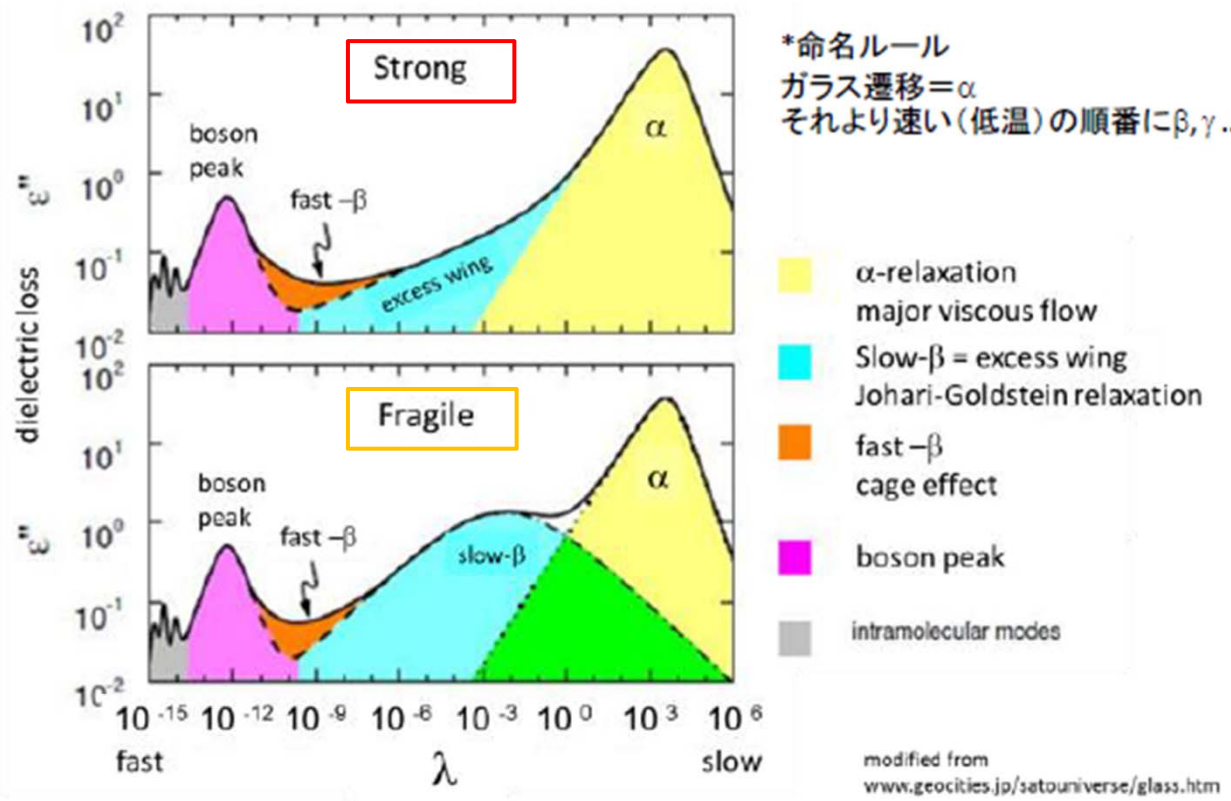

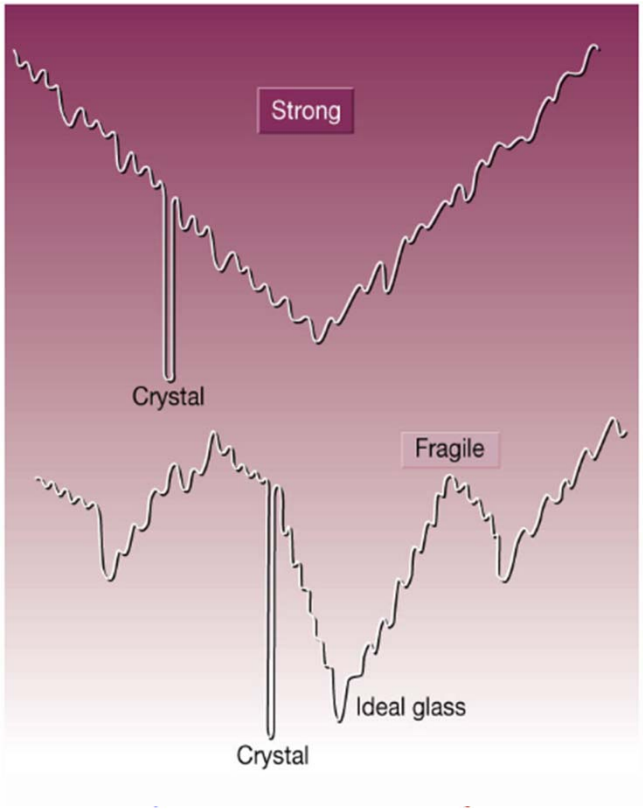

Strong: small deviation of activation E
between α relaxation and β relaxation

Fragile: large deviation of activation E
between α relaxation and β relaxation

Schematic representation of the energy landscapes of strong and fragile substances.

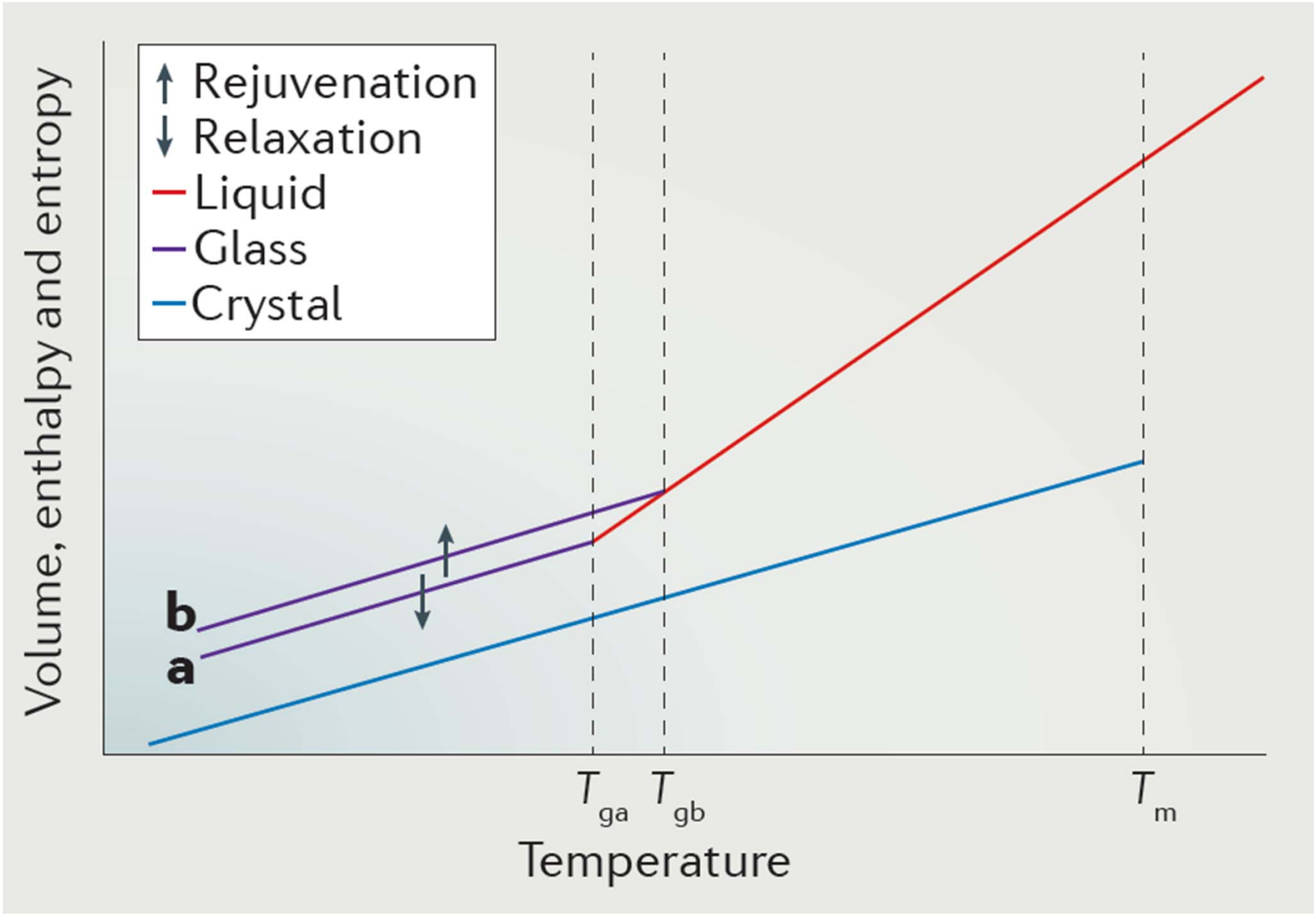
Rejuvenation
Relaxation
Liquid
Glass
Crystal
Volume, enthalpy and entropy
b
a
T_{ga}
T_{gb}
T_m
Temperature

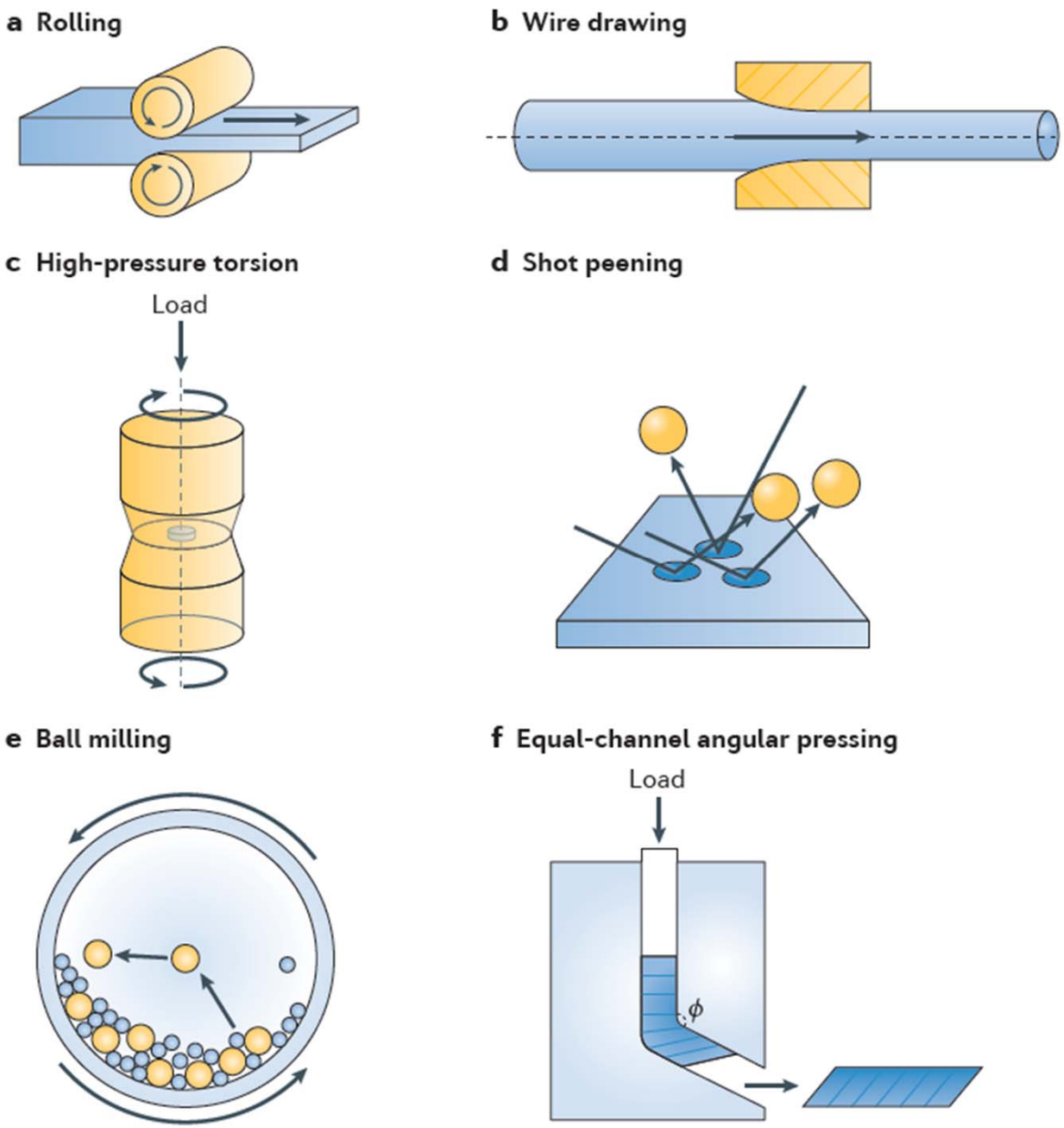
a Rolling
b Wire drawing
c High-pressure torsion
Load
d Shot peening
e Ball milling
f Equal-channel angular pressing
Load
ϕ

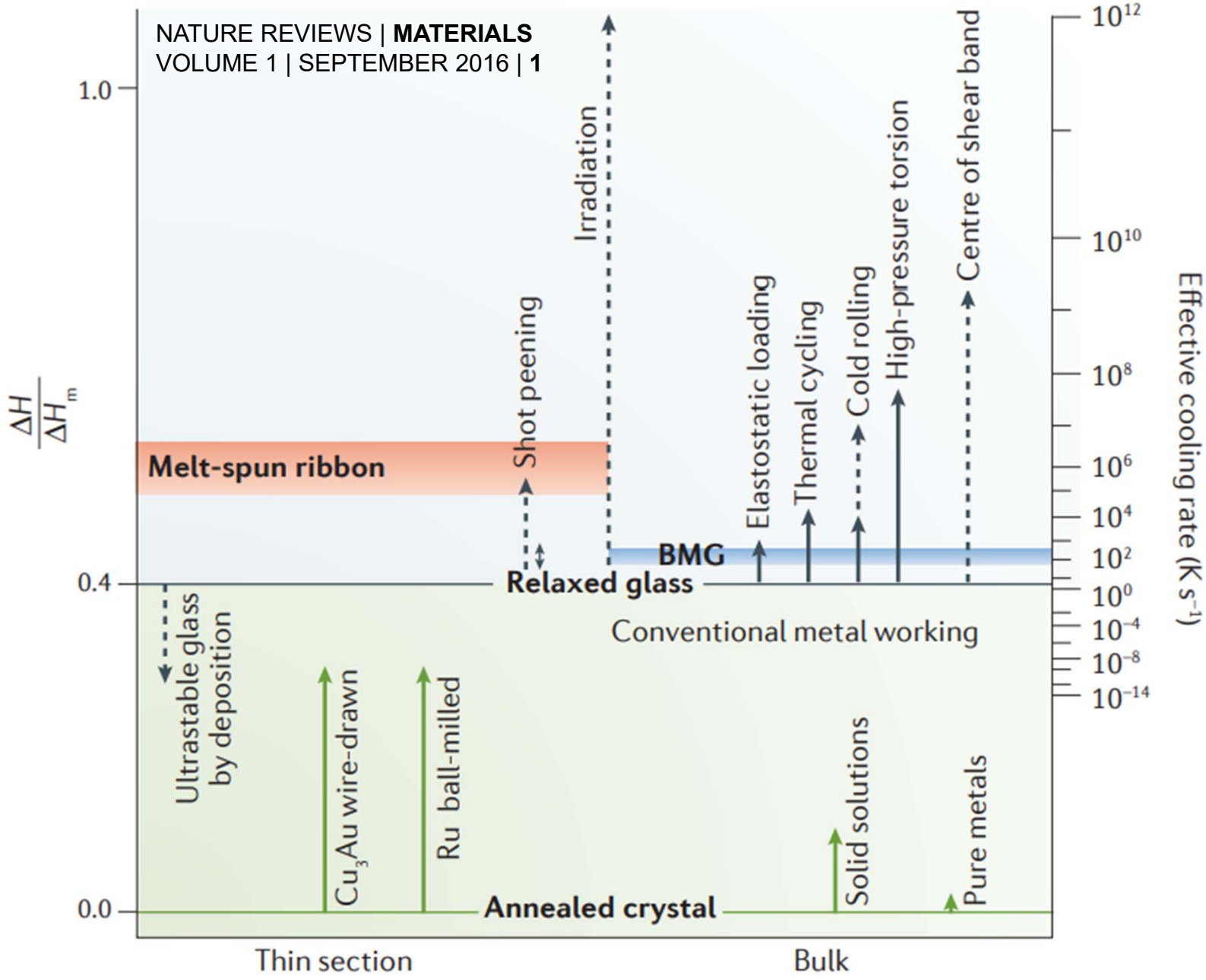

Figure 3 | **Relative enthalpies of deformed metallic states at room temperature.**

* Assuming that the change in enthalpy is entirely due to structural changes in the glassy state and that the average free volume per atom (=V_f/V_m, where V_f is the free volume and V_m is the atomic volume) is proportional to the change in enthalpy:

$$\frac{V_f}{V_m} = C\Delta H \tag{5.5}$$

where C is a constant. The proportionality constant C is determined by first calculating V_f using the Grest and Cohen model [83]:

$$V_f = \frac{k}{2s_0}\left(T - T_0 + \sqrt{(T-T_0)^2 + \frac{4V_a s_0}{k}T}\right) \tag{5.6}$$

$Zr_{44}Ti_{11}Ni_{10}Cu_{10}Be_{25}$ glassy

where k is the Boltzmann constant. The appropriate fit parameters for the above alloy were reported to be: $bV_m s_0/k = 4933\,\mathrm{K}$ with $b = 0.105$, $4V_a s_0/k = 162\,\mathrm{K}$, $T_0 = 672\,\mathrm{K}$. V_m for this alloy has been reported to be 1.67×10^{-29} m^3 near the liquidus temperature. Thus, by calculating V_f from Equation 5.6, V_f/V_m can be calculated.

→ The mechanical properties of metallic glasses (including the BMGs) are affected by the magnitude of free volume present in them. Hence, it becomes important to be able to quantitatively determine the free volume present in the glass to relate the magnitude of free volume to the changes in mechanical properties.

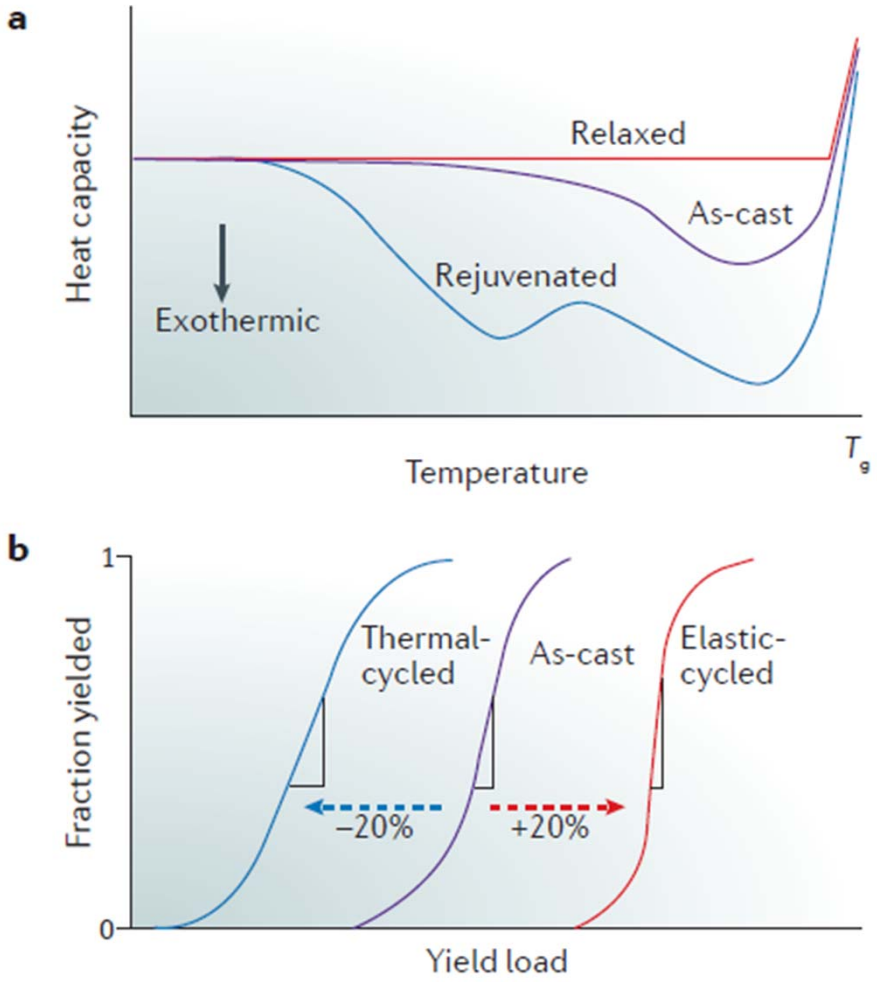
a
Heat capacity
Relaxed
As-cast
Rejuvenated
Exothermic
Temperature
T_g
b
1
0
Fraction yielded
Thermal-cycled
As-cast
Elastic-cycled
−20%
+20%
Yield load

Box 2 | **Energetic processing of metals**

The mechanical deformation of solids transfers energy to the material. This energy transfer also occurs in other processing methods including irradiation. Energetic processing of this type can lead to an energy increase in the sample (rejuvenation) but also to relaxation. These opposing trends are important for metallic glasses, which show a range of energies in their as-cast state (BOX 1). After long processing times, the changes induced in the structure and properties of the solid eventually saturate. More specifically, a steady state is reached in which the rate of structural change (damage) introduced by the processing is balanced by the rate of structural relaxation, which is enhanced by the increased atomic mobility in the processed material. In the steady state, enthalpy, entropy and volume are higher — that is, the state is less relaxed and more rejuvenated — at higher processing rates (strain rate or irradiation flux) and at lower temperatures. This reflects the balance of damage and relaxation rates.

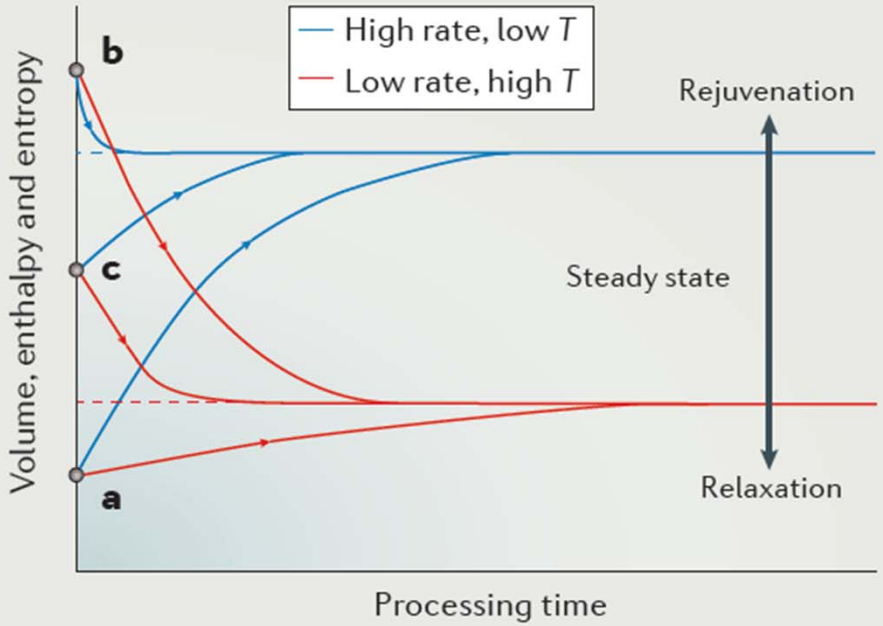

The illustration shows three possible cases: case **a** is a solid of low initial energy (for example, a polycrystal with a low dislocation density or a relaxed glass) that retains some of the injected energy and evolves into a more rejuvenated state; case **b** is a solid of high initial energy (for example, a polycrystal with a high dislocation density or a rapidly quenched glass) that evolves into a more relaxed state; and case **c** is a given initial state that may evolve in either direction, depending on processing rate and temperature. Such considerations, which are well understood for mechanical deformation[52] and irradiation[145] of polycrystalline metals, need to be further explored in the context of the mechanical deformation of metallic glasses.

Annealing of Bulk Metallic Glasses: SR → SCLR (& PS) → Crystallization

5.7.2 Glass Transition: abrupt variation of C_p

Acta Materialia 59 (2011)

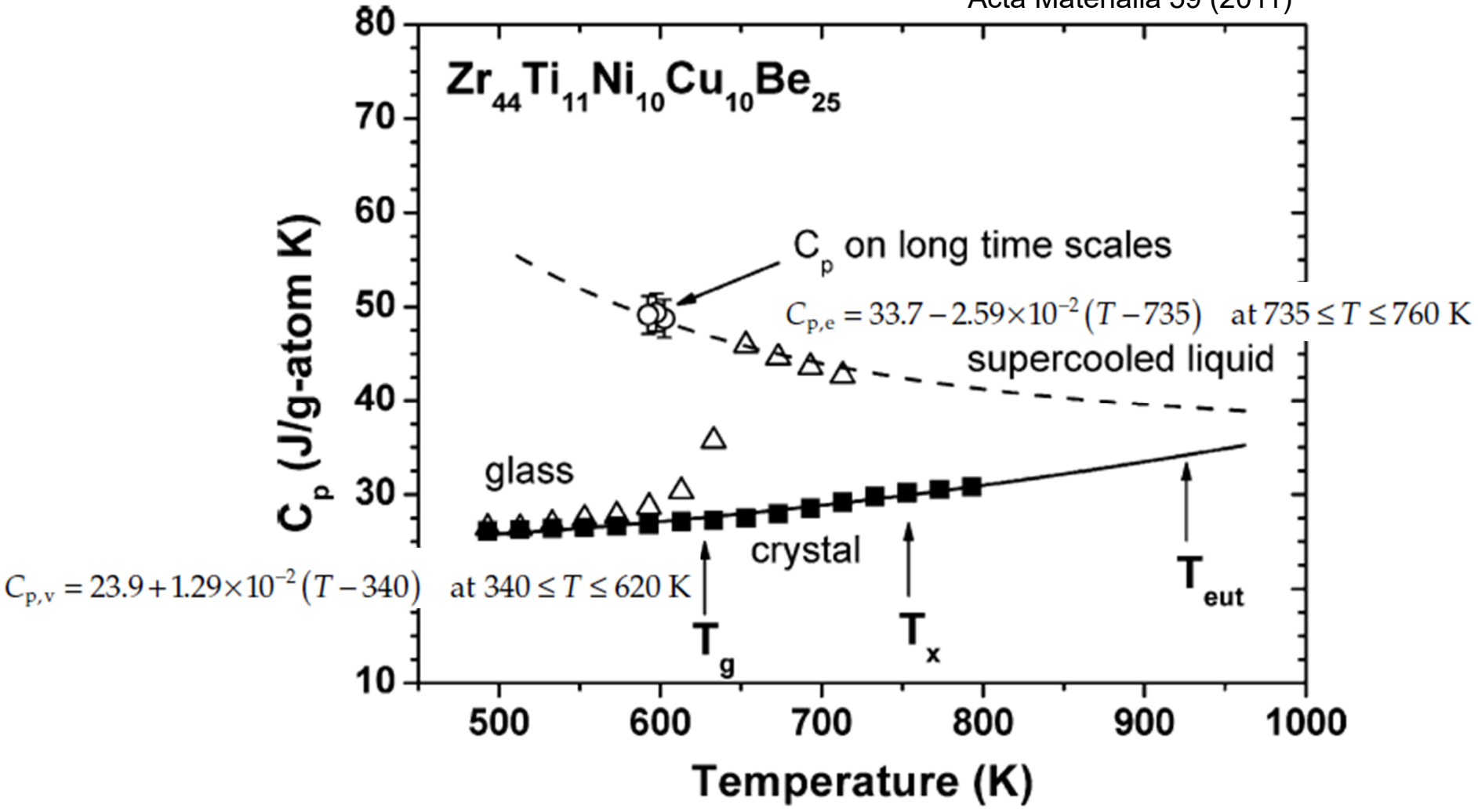

- **Ideal glass transition temperature (T_{oc} =T_g^0)**

: lower temperature limit to occur glass transition thermodynamically

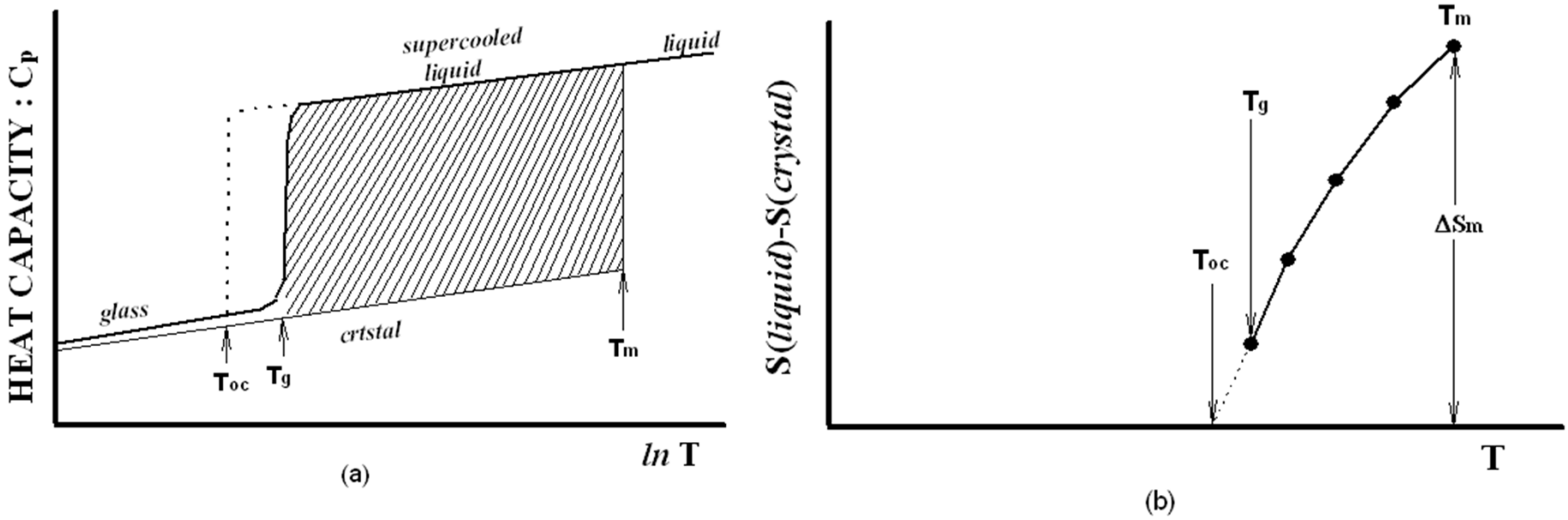

Variation of (a) C_p and (b) excess entropy, S depending on temp. for glass, crystal and liquid. Ideal glass transition temp, T_{oc}. is the temperature when excess entropy is disappeared.

TABLE 5.4

Increase in Specific Heat from the As-Quenched Glassy (g) State to the Supercooled Liquid (scl) Condition, $\Delta C_{p,g\rightarrow scl}$ for Different Metallic Glasses Synthesized by Melt Spinning, and Measured at a Heating Rate of 0.67 K s^{-1} (40 K min^{-1})

Composition	$\Delta C_{p,g\rightarrow scl}$ (J mol^{-1} K^{-1})	ΔT_x (K)	Reference
$La_{55}Al_{20}Cu_{25}$	11.5	59	[84]
$La_{55}Al_{25}Ni_{20}$	14.0	69	[85]
$Mg_{50}Ni_{30}La_{20}$	17.4	58	[86]
$Zr_{60}Al_{15}Ni_{25}$	6.25	77	[87]
$Zr_{65}Cu_{27.5}Al_{7.5}$	—	88	[75]
$Zr_{65}Cu_{17.5}Ni_{10}Al_{7.5}$	14.5	127	[15]

Note: ΔT_x represents the width of the supercooled liquid region.

The $\Delta C_{p,g\rightarrow scl}$ values for the Zr-based metallic glasses are considerably smaller than those of Pd–Ni–P and Pt–Ni–P glasses. Even though the reasons for this difference are not clearly known at the moment, it is possible that it is related to (1) the higher packing fraction of atoms in the glassy Zr-alloys, which require a lower cooling rate to form the glassy structure, (2) the possibility of the atomic configuration in the glassy and supercooled liquid structures being similar, and (3) the higher T_g values in comparison to those of La-, Mg-, Pd-, and Pt-based glassy alloys.

Overshoot in heating process

When the kinetics become fast enough to allow the sample to regain metastable equilibrium

Determined from DSC up-scan

$$\int_{T^*}^{T_f'} (C_p^e - C_p^g) dT_f = \int_{T^*}^{T'} (C_p - C_p^g) dT$$

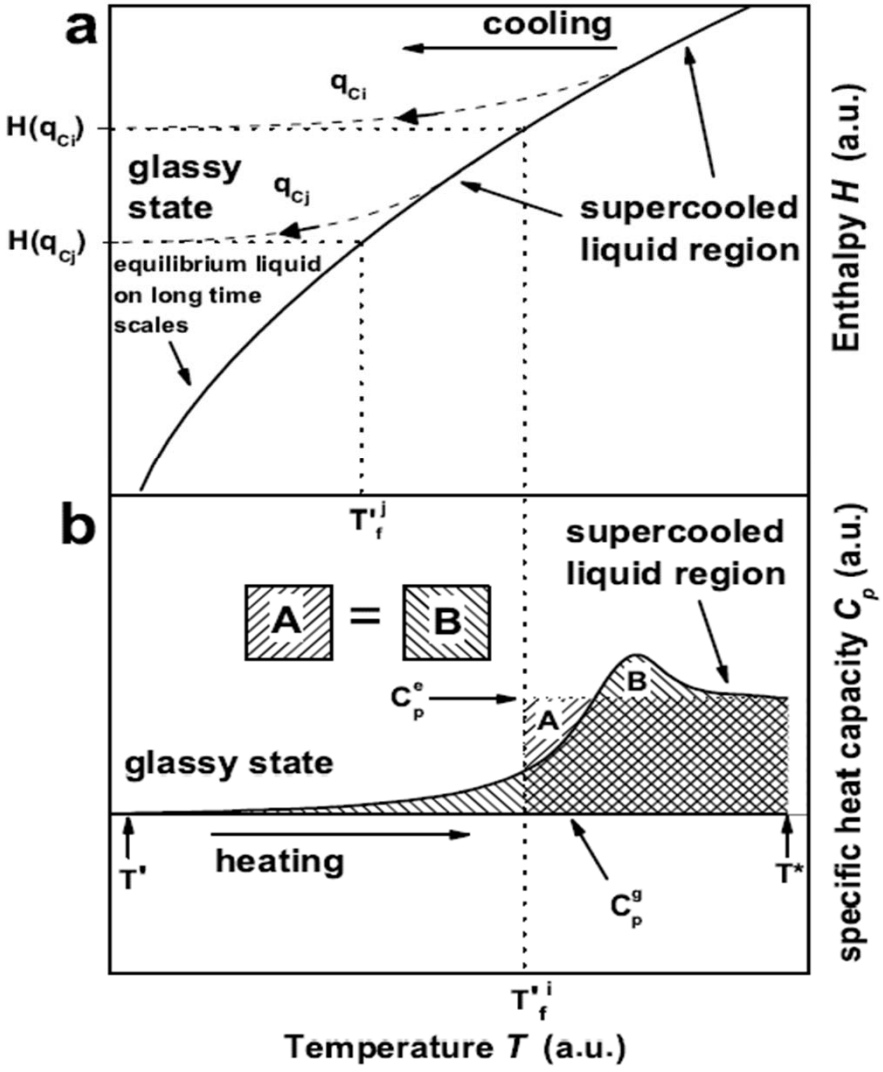

J. Appl. Phys. 107, 123529 (2010)

5.7.3 Phase separation

2-Amorphous phases

Polymer

(AFM)
PGMA/PS

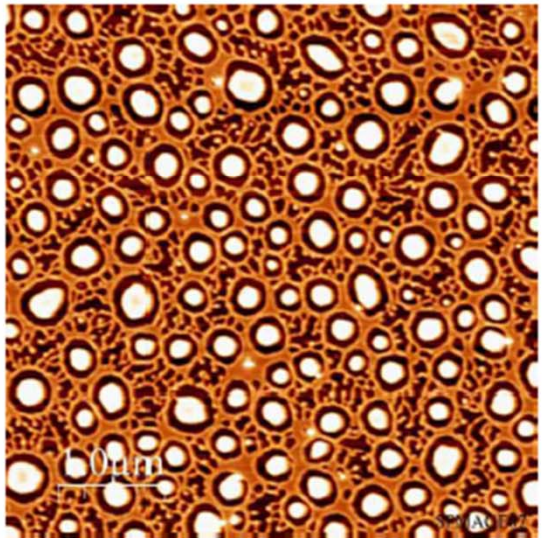

Oxide glass

(SEM)
SiO_2-NaO_2

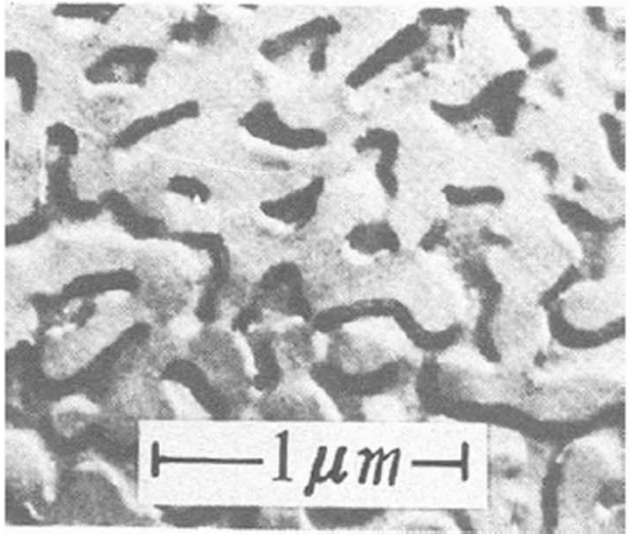

Metallic glass

(TEM)
TiYAlCo

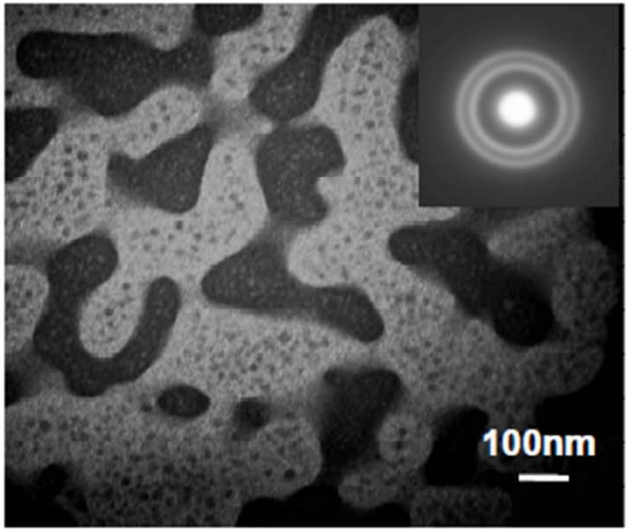

Annealing of Bulk Metallic Glasses: SR → SCLR (& PS) → Crystallization

5.7.3 Phase separation

* Miscibility gaps in phase separating system

- **Stable immiscibility**

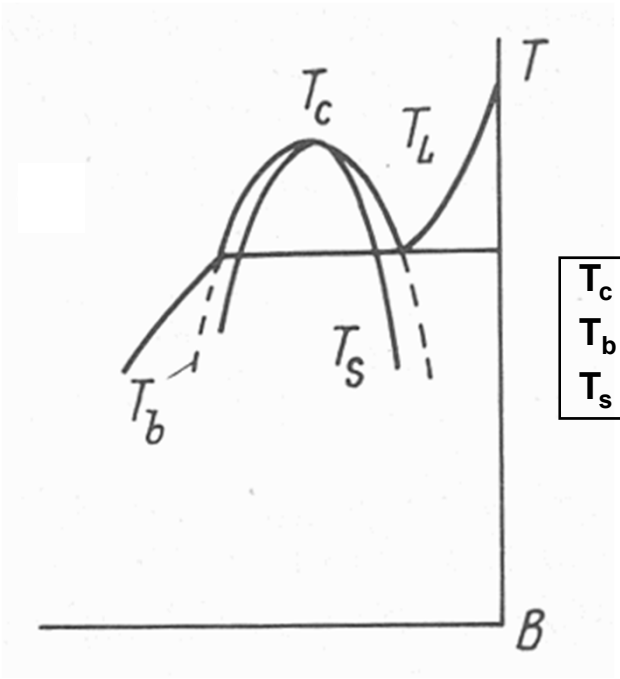

T_c : critical temperature
T_b : binodal curve
T_s : spinodal curve

immiscibility above the liquidus

⇒ decomposition into stable liquid

- **Metastable immiscibility**

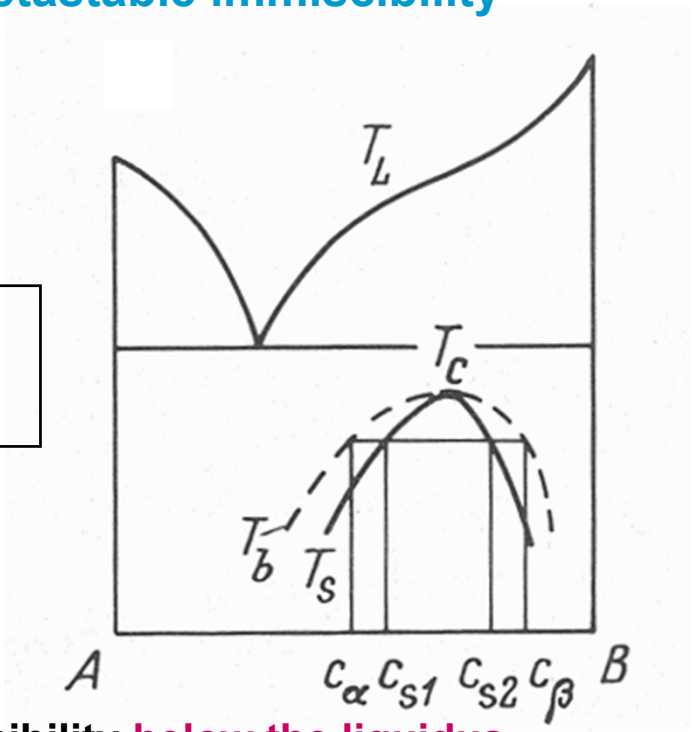

immiscibility below the liquidus

⇒ decomposition into metastable liquid

"Phase separation in glass" ed. by Mazurin and Porai-Koshits (1984)

(a) Positive heat of mixing relation among constituent elements

- **Alloy design considering heat of mixing relation among constituent elements**

$\Delta H_{mix} \gg 0$ between A & B

⬇

creates (meta)stable miscibility gap in limited composition range

⬇

Phase separation to A-rich & B-rich phase

- **Different two-phase structure by initial composition before phase separation**

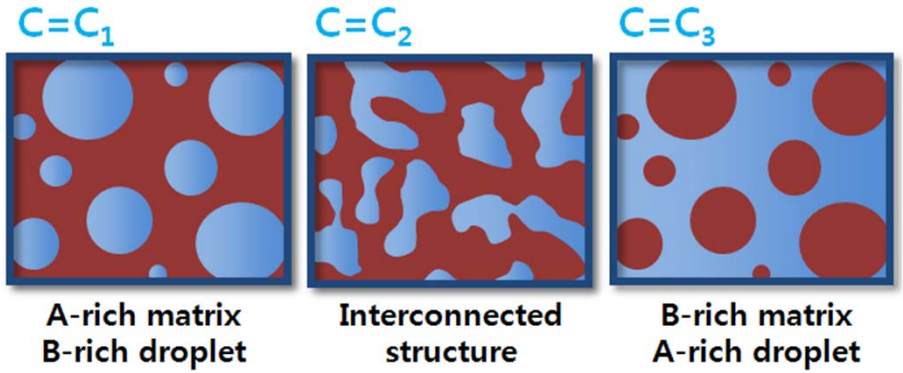

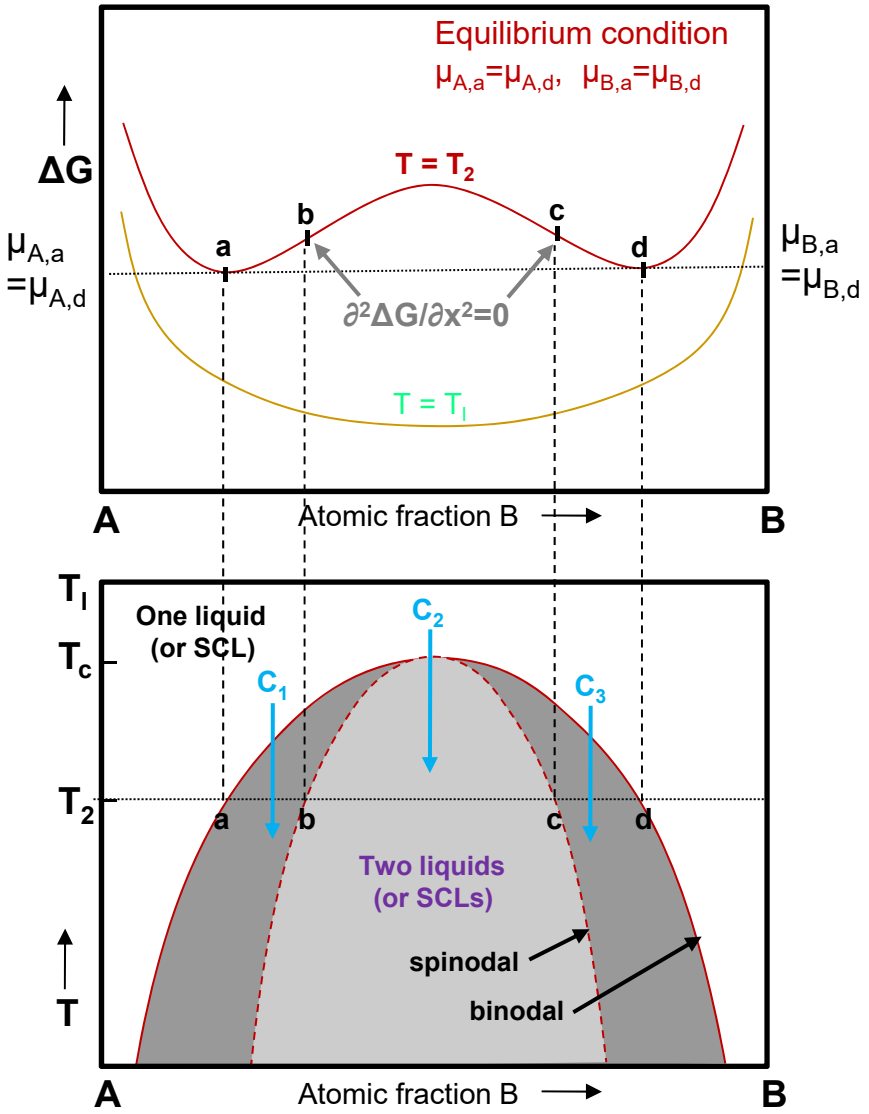

Nucleation and growth ↔ Spinodal decomposition without any barrier to the nucleation process

3D image construction process - $Gd_{30}Ti_{25}Al_{25}Co_{20}$

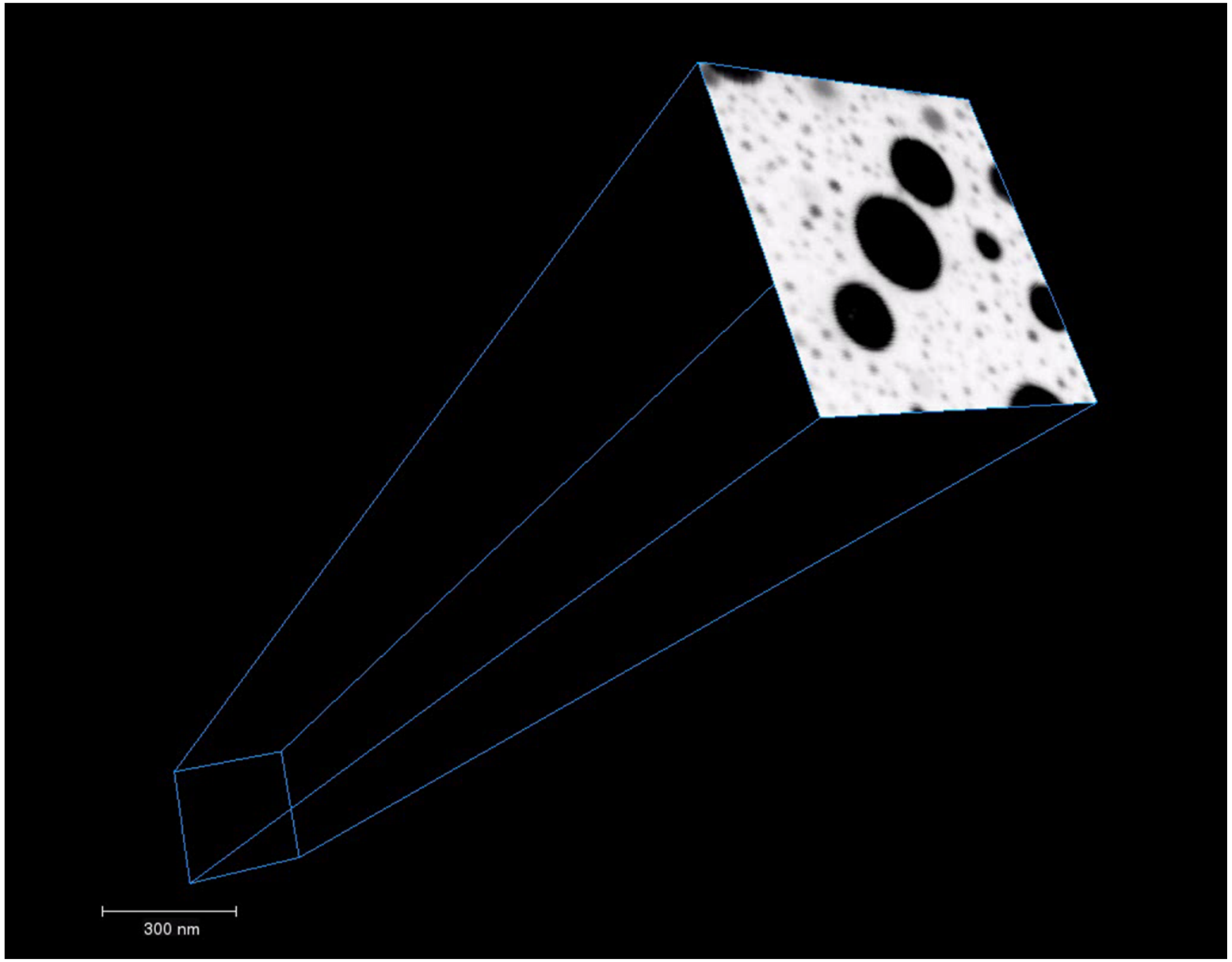

3D microstructure of phase separated metallic glass

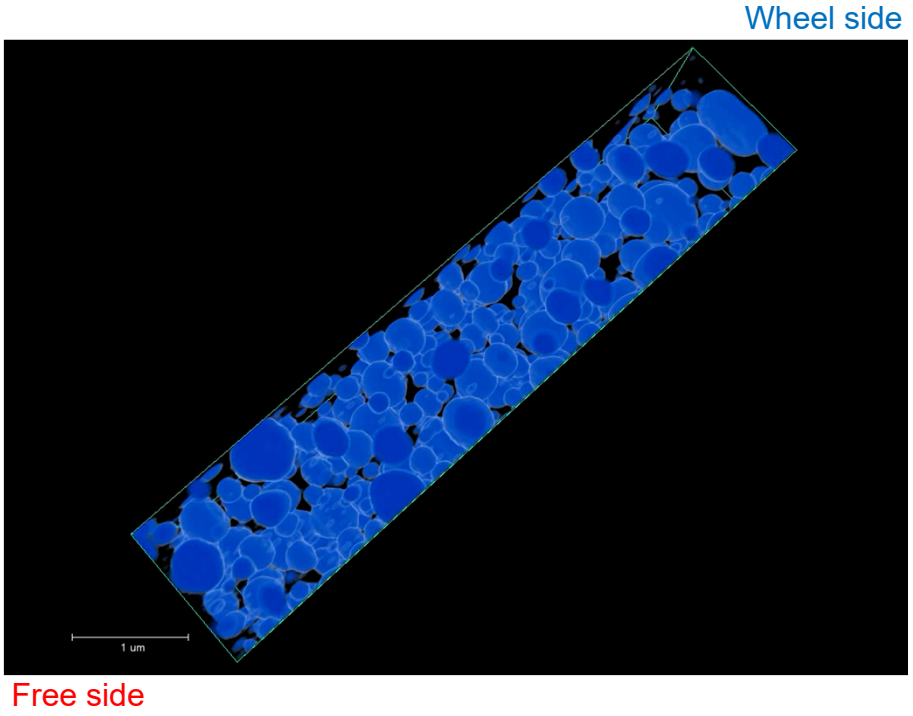

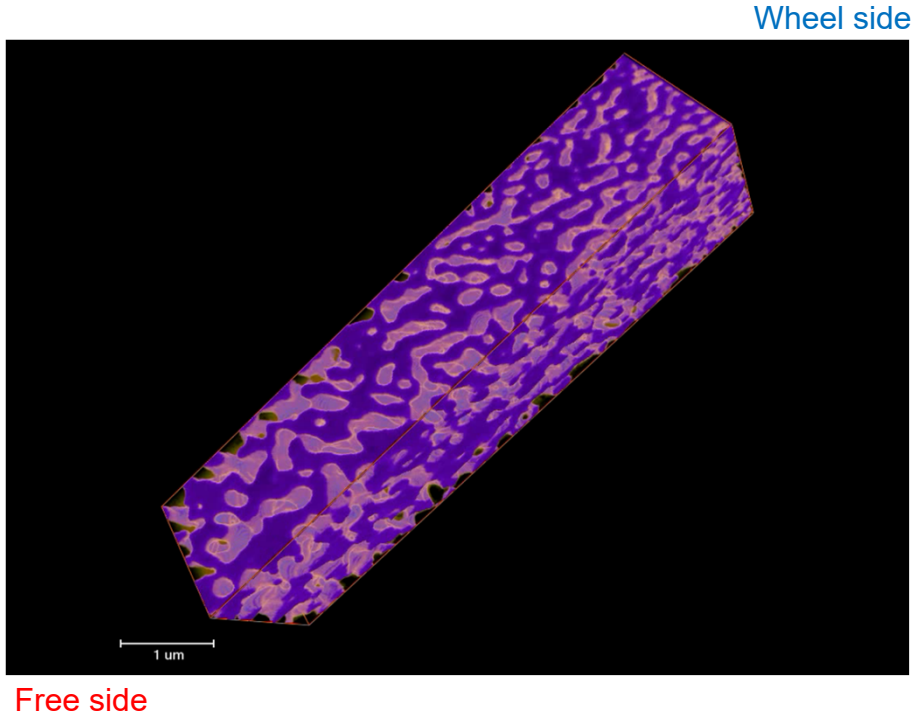

Volume fraction = 33.78%

Volume fraction = 48.74%

It is possible to tailor the sizes of the glassy phases by varying the solidification rate during cooling.

5.5.5 Spinodal Decomposition

Spinodal mode of transformation has no barrier to nucleation

: describing the transformation of a system of two or more components in a metastable phase into two stable phases

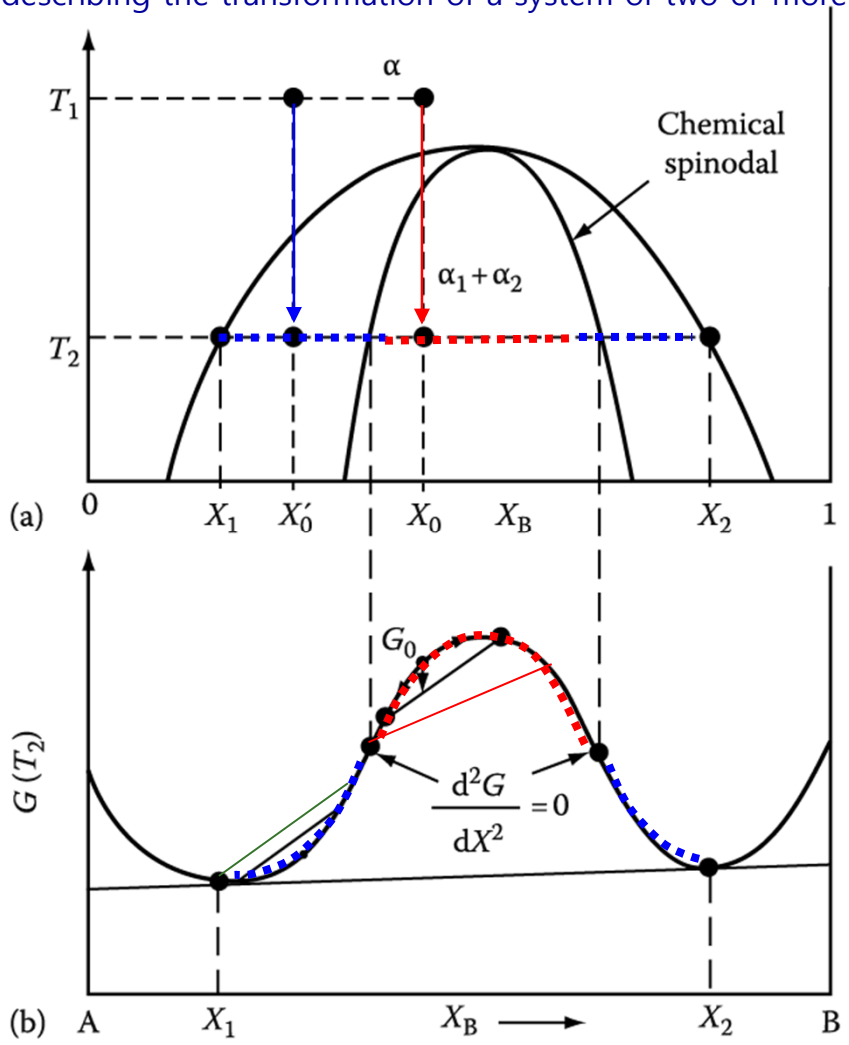

Fig. 5.38 Alloys between the spinodal points are unstable and can decompose into two coherent phasees α_1 and α_2 without overcoming an activation energy barrier. Alloys between the coherent miscibility gaps and the spinodal are metastable and can decompose only after nucleation of the other phase.

How does it differ between inside and outside the inflection point of Gibbs free energy curve?

1) Within the spinodal $\frac{d^2G}{dX^2} < 0$

: phase separation by small fluctuations in composition/ **"up-hill diffusion"**

2) If the alloy lies outside the spinodal, small variation in composition leads to an increase in free energy and the alloy is therefore metastable.

The free energy can only be decreased if nuclei are formed with a composition very different from the matrix.

→ nucleation and growth
: "down-hill diffusion"

a) Composition fluctuations within the spinodal

b) Normal down-hill diffusion outside the spinodal

up-hill diffusion

down-hill diffusion

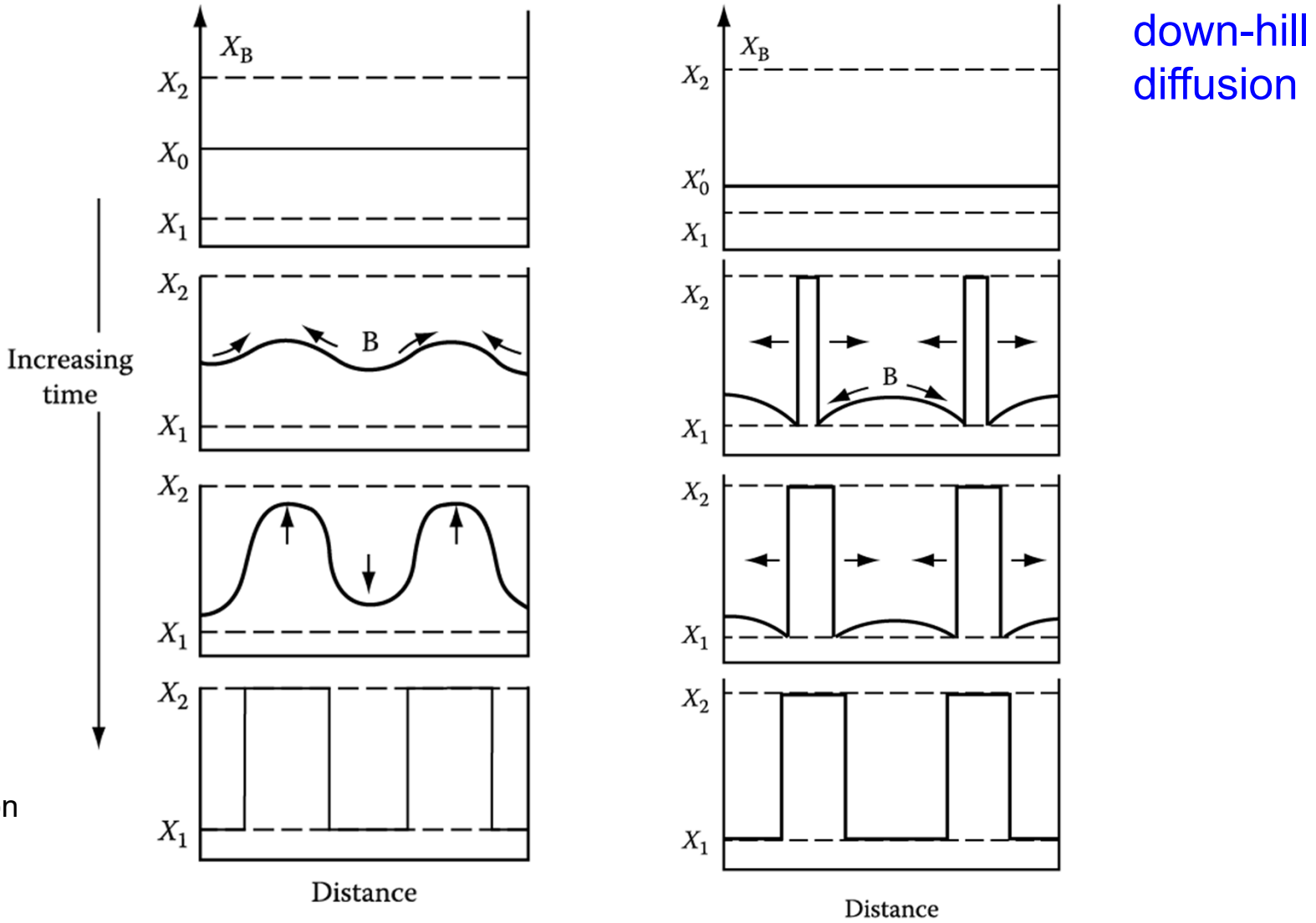

interdiffusion coefficient D<0

Fig. 5.39 & 5.40 schematic composition profiles at increasing times in (a) an alloy quenched into the spinodal region (X_0 in Figure 5.38) and (b) an alloy outside the spinodal points (X_0' in Figure 5.38)

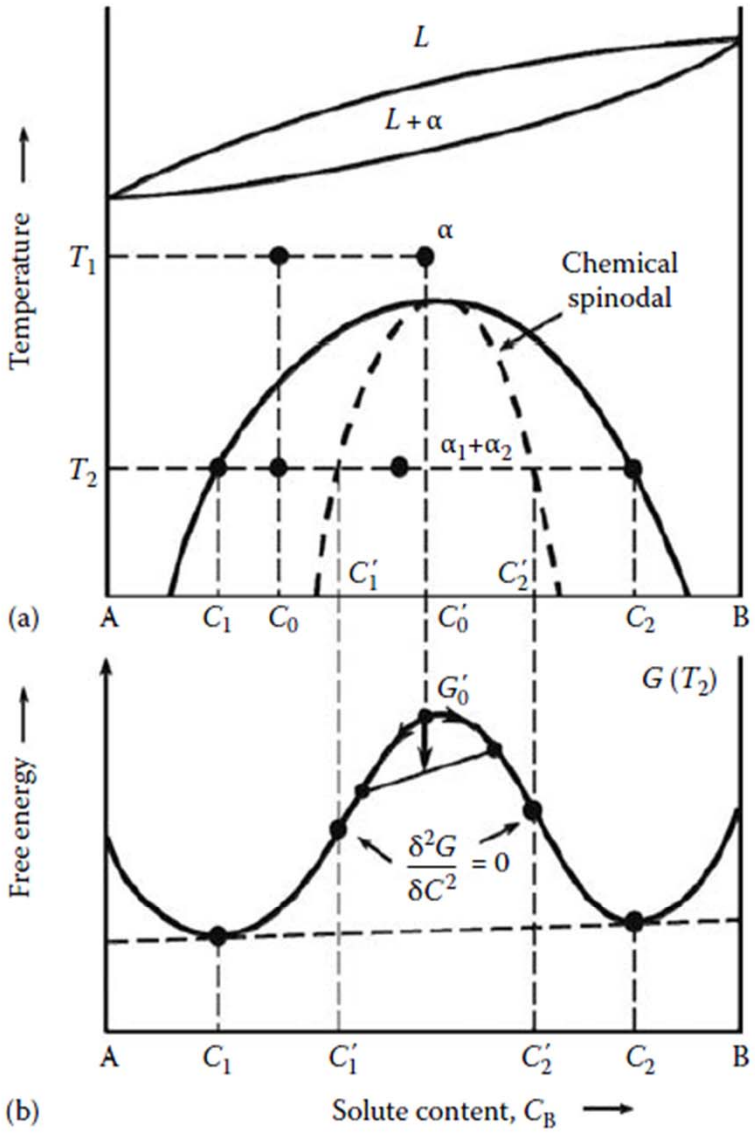

FIGURE 5.14
(a) Typical phase diagram showing a miscibility gap in the solid state. (b) The corresponding free-energy vs. composition diagram featuring two minima. Phase separation is possible in such an alloy system either by a nucleation and growth process or by a spinodal decomposition process.

TABLE 5.5

Alloy Systems Showing Phase Separation in the Glassy State

Alloy Composition	Synthesis Method	Characterization Method(s)	Compositions of the Two Glassy Phases	Comments	References
$Ag_{20}Cu_{48}Zr_{32}$	Melt spinning	TEM			[93]
$Cu_{43}Zr_{43}Al_7Ag_7$	Cu-mold casting	TEM and 3DAP	$Cu_{40.7}Zr_{46.8}Al_{8.0}Ag_{4.5}$ and $Cu_{36.8}Zr_{43.5}Al_{7.0}Ag_{12.7}$	Phase separation due to unusually high plastic strain	[94]
$Cu_{46}Zr_{22}Y_{25}Al_7$	Melt spinning	DSC and TEM	$Cu_{35.7}Zr_{12.8}Y_{44.3}Al_{7.2}$ and $Cu_{53.4}Zr_{31.8}Y_{8.3}Al_{6.5}$		[95]
$La_{27.5}Zr_{27.5}Al_{25}Cu_{10}Ni_{10}$	Melt spinning	SEM and TEM	$La_{5.0}Zr_{51.4}Cu_{5.4}Ni_{13.2}Al_{25}$ and $La_{43.4}Zr_{10.9}Cu_{14.4}Ni_{8.2}Al_{22.1}$		[96]
$Nd_{60-x}Zr_xAl_{10}Co_{30}$ $(6 \le x \le 40)$	Melt spinning	DSC and TEM			[97]
$Ni_{70}Nb_{15}Y_{15}$	Melt spinning	DSC, TEM, and SAXS			[98]
$Ni_{66}Nb_{17}Y_{17}$	Melt spinning	DSC, TEM, and SAXS			[98]
$Ni_{58.5}Nb_{20.25}Y_{21.25}$	Melt spinning	DSC, SEM, TEM, and SAXS	$Ni_{59}Nb_{16}Y_{25}$ and $Ni_{57}Nb_{28}Y_{15}$ by SEM and $Ni_{53}Nb_{42}Y_5$ and $Ni_{60}Nb_{10}Y_{30}$ by TEM	No two T_gs were observed	[98,99]
$Ni_{54}Nb_{23}Y_{23}$	Melt spinning	DSC, TEM, and SAXS	$Ni_{50}Nb_{44}Y_6$ and $Ni_{58}Nb_7Y_{35}$		[98]
$Ni_{61}Zr_{28-x}Nb_7Al_4Ta_x$ $(x=0, 2, 4, 6, 8)$	Melt spinning			No evidence of phase separation	[100]
$Pd_{80}Au_{3.5}Si_{16.5}$	Roller quenching	DSC and SAXS		Apparent phase separation	[31]
$Pd_{78}Au_6Si_{16}$	Splat cooling	DSC and TEM	Segregation into (Pd–Au)-rich and Si-rich glassy phases	No clear identification of the phases	[30]
$Pd_{40.5}Ni_{40.5}P_{19}$	Centrifugal spinning	DSC		Two T_gs were observed only after the original glassy sample was heated beyond the first exothermic peak, then cooled quickly and reheated	[34]

TABLE 5.5 (continued)

Alloy Systems Showing Phase Separation in the Glassy State

Alloy Composition	Synthesis Method	Characterization Method(s)	Compositions of the Two Glassy Phases	Comments	References
$Pd_{80}Si_{20}$	Splat cooling	DSC and TEM	Pd-rich particles embedded in a Si-rich matrix	No clear identification of the phases	[30]
$Ti_{28}Y_{28}Al_{24}Co_{20}$	Melt spinning	XRD and TEM	$Y_{40.4}Ti_{14.7}Al_{21.9}Co_{23}$ and $Ti_{45.6}Y_{11.6}Al_{26.7}Co_{16.1}$	No clear T_g in DSC	[101]
$Ti_{56-x}Y_xAl_{22}Co_{22}$ ($x = 11$, 20, or 28)	Melt spinning	TEM	$Y_{44.5}Ti_{8.8}Al_{36.9}Co_{9.8}$ and $Ti_{47.2}Y_{2.1}Al_{19.9}Co_{30.8}$. These compositions depend on the initial composition of the alloy.		[102]
$Zr_{63.8}Ni_{16.2}Cu_{15}Al_5$	Cu-mold casting		$Zr_{68.5}Cu_{8.1}Ni_{21.3}Al_{2.1}$ and $Zr_{62.4}Cu_{16.7}Ni_{14.6}Al_{6.3}$	Noted 30% plastic strain during compression at room temperature	[103]
$Zr_{36}Ti_{24}Be_{40}$	Melt spinning	DSC and TEM		Two T_gs were reported. Nagahama et al. [104] concluded that this alloy crystallized in a eutectic mode and that there was no phase separation	[89]
$Zr_{52.5}Ti_5Cu_{17.9}Ni_{14.6}Al_{10}$ (Vit 105)	Cu-mold casting and Melt spinning	SANS and TEM		Phase separation? Kajiwara et al. [106] suggested primary crystallization	[105]
$Zr_{41.2}Ti_{13.8}Cu_{12.5}Ni_{10.0}Be_{22.5}$ (Vit 1)	Water quenching	DSC, SANS, TEM and APFIM	Zr-rich and Be-rich phases		[107–109]
$Zr_{28}Y_{28}Al_{22}Co_{22}$	Melt spinning	Dynamic Mechanical Analysis and TEM	$Y_{30.9}Zr_{26.0}Al_{24.8}Co_{18.3}$ and $Zr_{36.4}Y_{15.8}Al_{28.8}Co_{19.0}$	Phase separation observed during heating of a homogeneous glassy phase	[110]
$Zr_{60-x}Y_xAl_{15}Ni_{25}$ ($x = 15$, 27, and 45)	Melt spinning	DSC		Two supercooled liquid regions	[111]

a. Phase separation in solid state

- Pd-Si-Ag alloy / two amorphous phase formation after heating just above T_g

Chen and Turnbull, Acta Metall., 17, 1021 (1969)

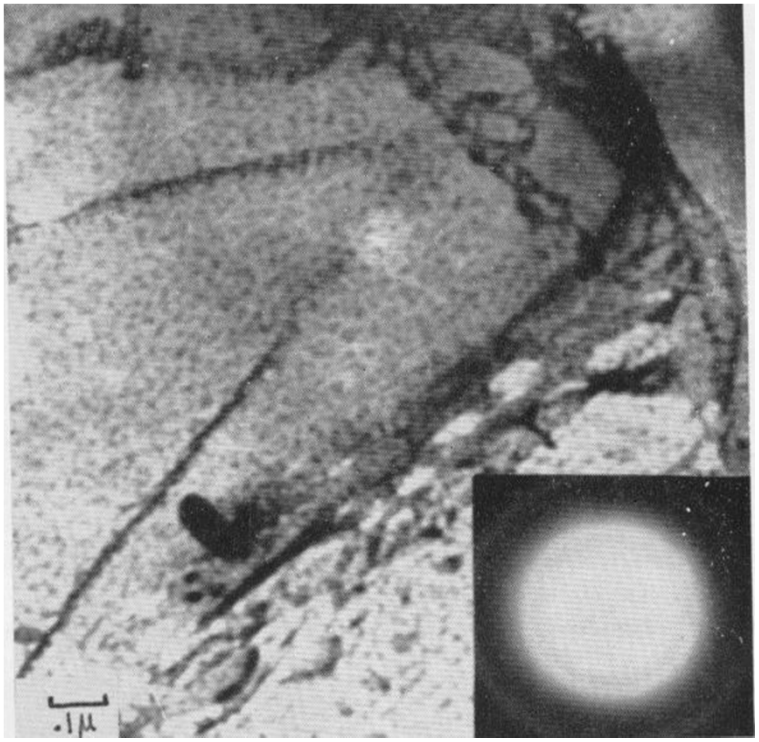

- After heating just above T_g, two amorphous separation occurs, but crystallization occurs simultaneously.

- Zr-Ti-Cu-Ni-Be BMG / small angle neutron scattering

Schneider et al, Appl. Phys. Lett., 68, 493 (1996)

decomposed during cooling in the liquid state to a two-phase mixture of Be-rich and Zr-rich glassy regions with a typical length scale of tens of nanometers

Martin et al., Acta Mater., 52, 4427 (2004)

Ti-rich and Be-depleted regions that appeared in the early stage of annealing due to the partitioning of alloying elements accompanied by the crystallization reaction.

* Zr-Y-Al-Ni system: homogeneous glassy phase in the as-quenched state had transformed into a mixed structure consisting of the Zr-rich Zr-Al-Ni glassy phase and the Y-rich Y-Al-Ni crystalline phase (3-5 nm).

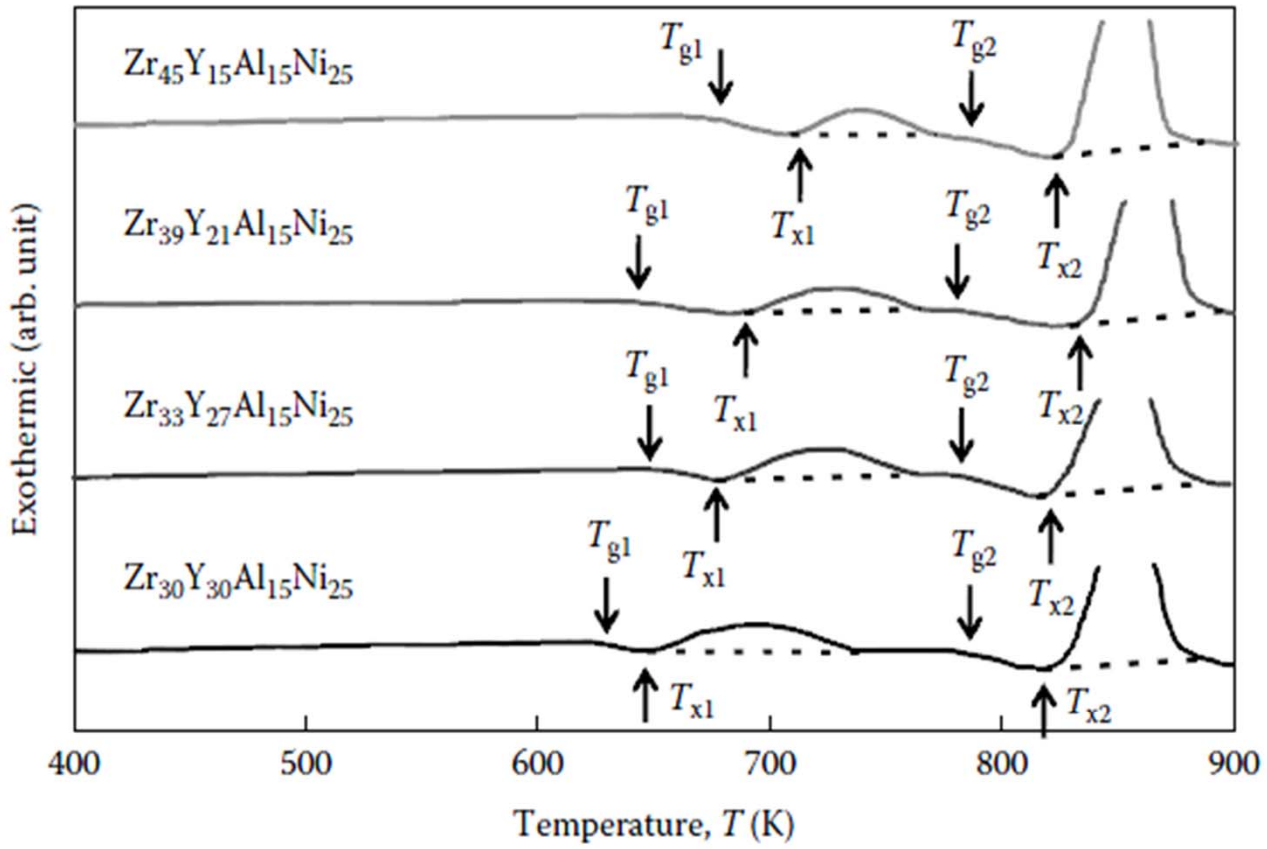

FIGURE 5.15
DSC curves of the glassy $Zr_{60-x}Y_xAl_{15}Ni_{25}$ (x=15, 21, 27 and 30) alloys obtained at a heating rate of 0.67 K s^{-1}(40 K min^{-1}). Note the presence of two T_gs and two T_xs in all the alloys studied. (Reprinted from Inoue, A. et al., *Mater. Sci. Eng. A*, 179/180, 346, 1994. With permission.)

* Zr-Y-Al-Ni system: exhibit two glass transition temperature

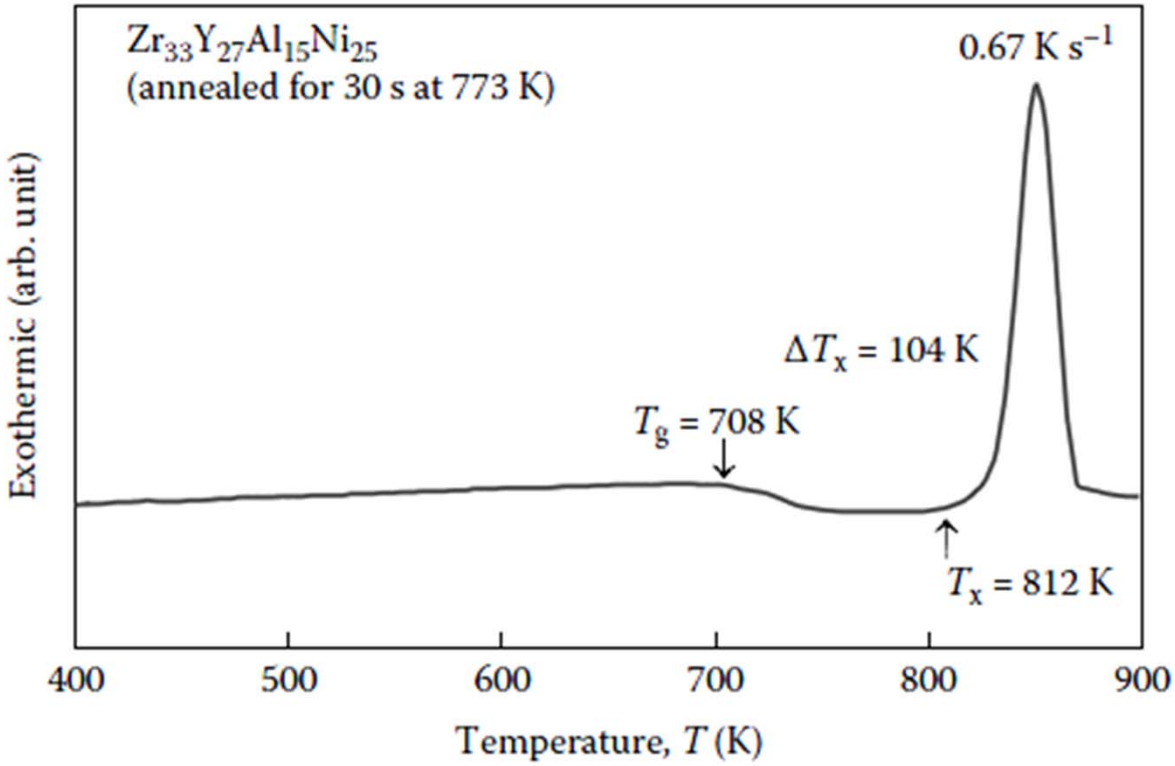

FIGURE 5.16
DSC curve of the glassy $Zr_{33}Y_{27}Al_{15}Ni_{25}$ alloy pre-annealed for 30 s at 773 K. The width of the supercooled liquid region, ΔT_x (= $T_x - T_g$), has now increased to 104 K from 40 K in the as-solidified condition. (Reprinted from Inoue, A. et al., *Mater. Sci. Eng. A*, 179/180, 346, 1994. With permission.)

b. Phase separation in liquid state

* La-Zr-Al-Cu-Ni system

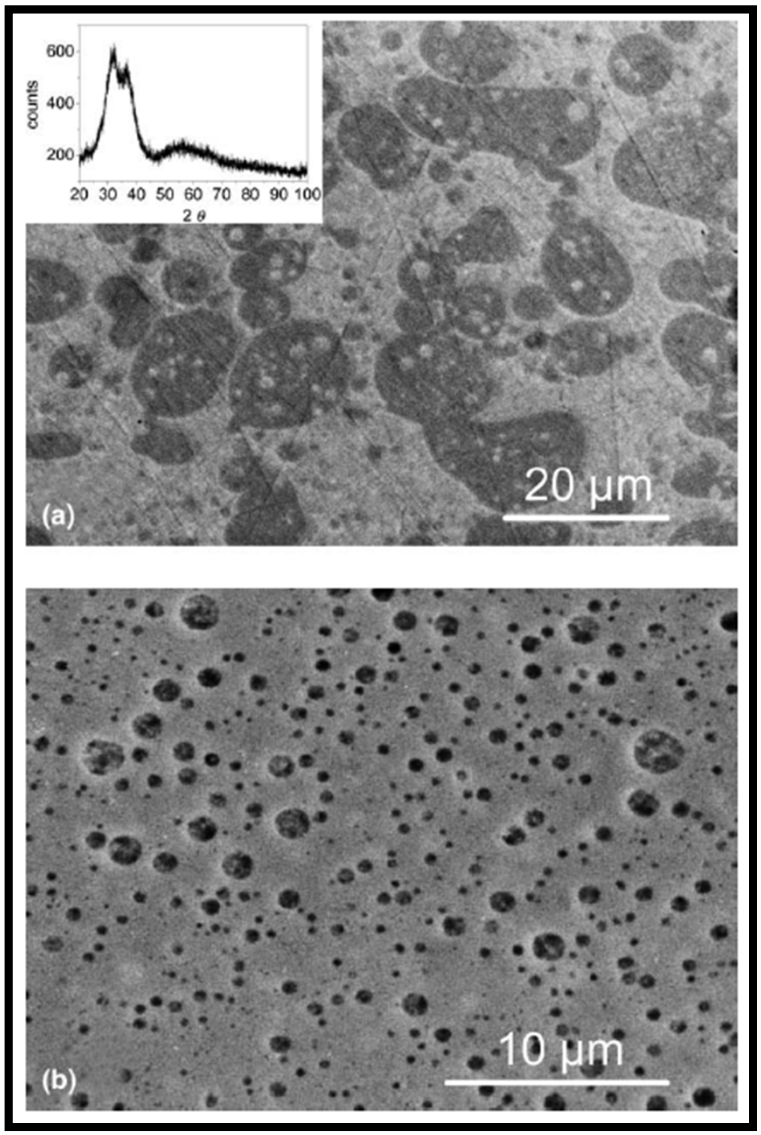

Kundig et al., *Acta Mat.*, 52 (2004) 2441-2448.

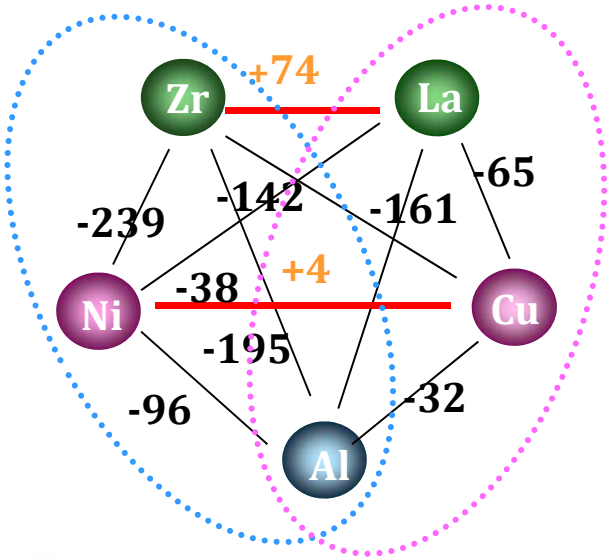

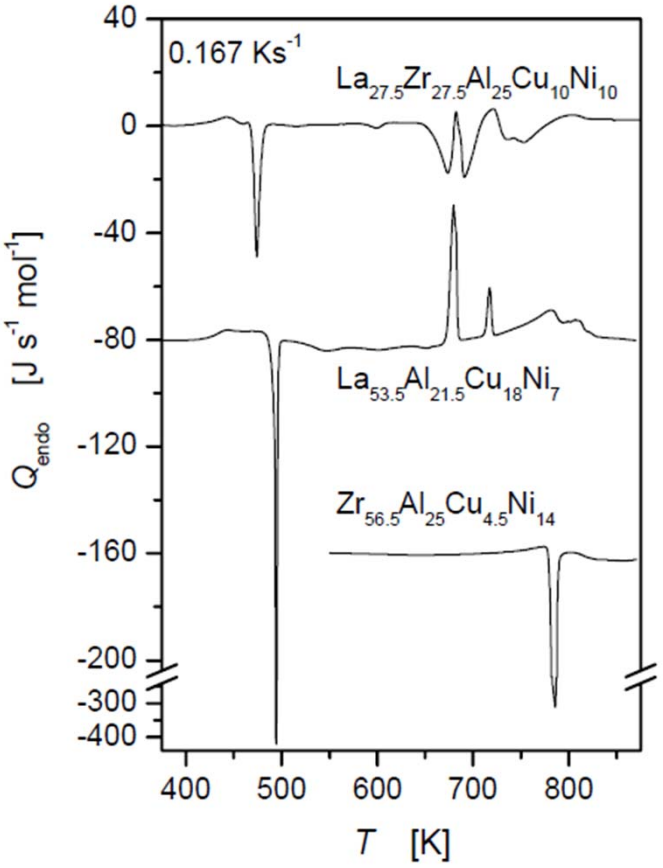

* La-Zr-Al-Cu-Ni system

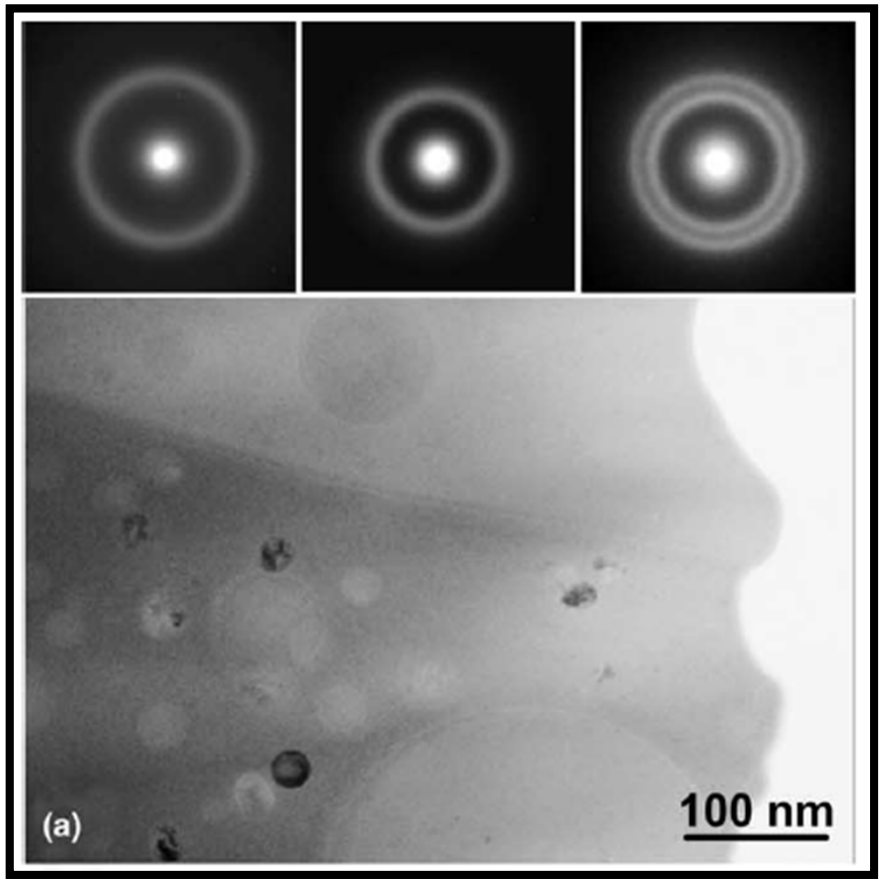

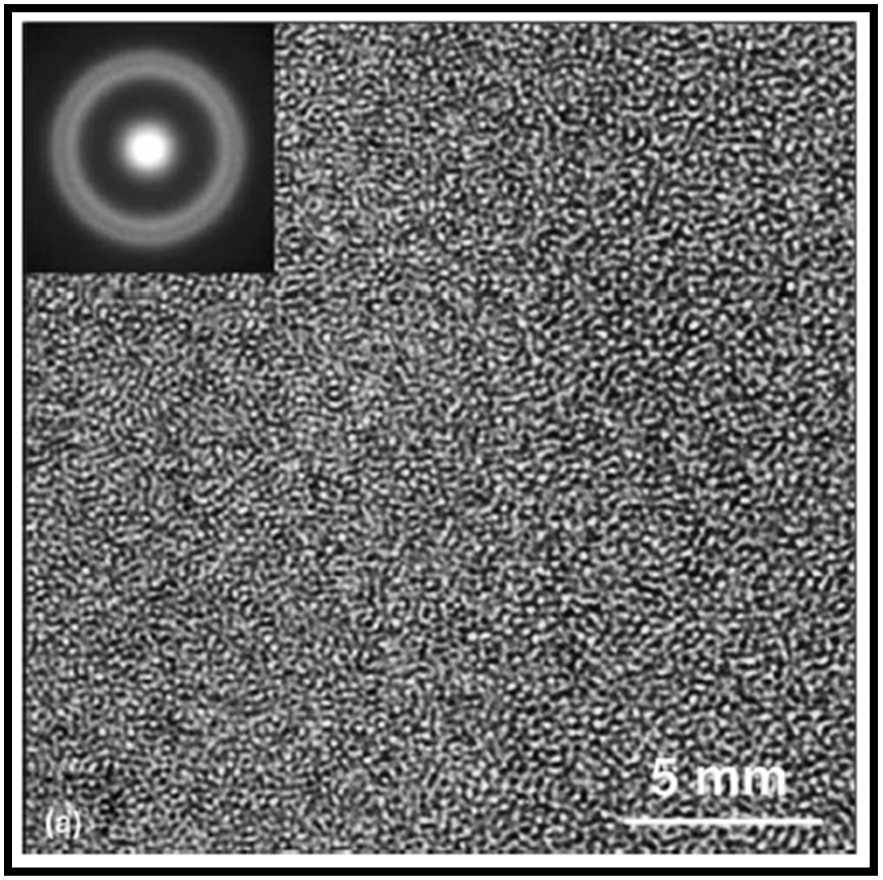

Kundig et al., *Acta Mat.*, 52 (2004) 2441-2448.

* La-Zr-Al-Cu-Ni system

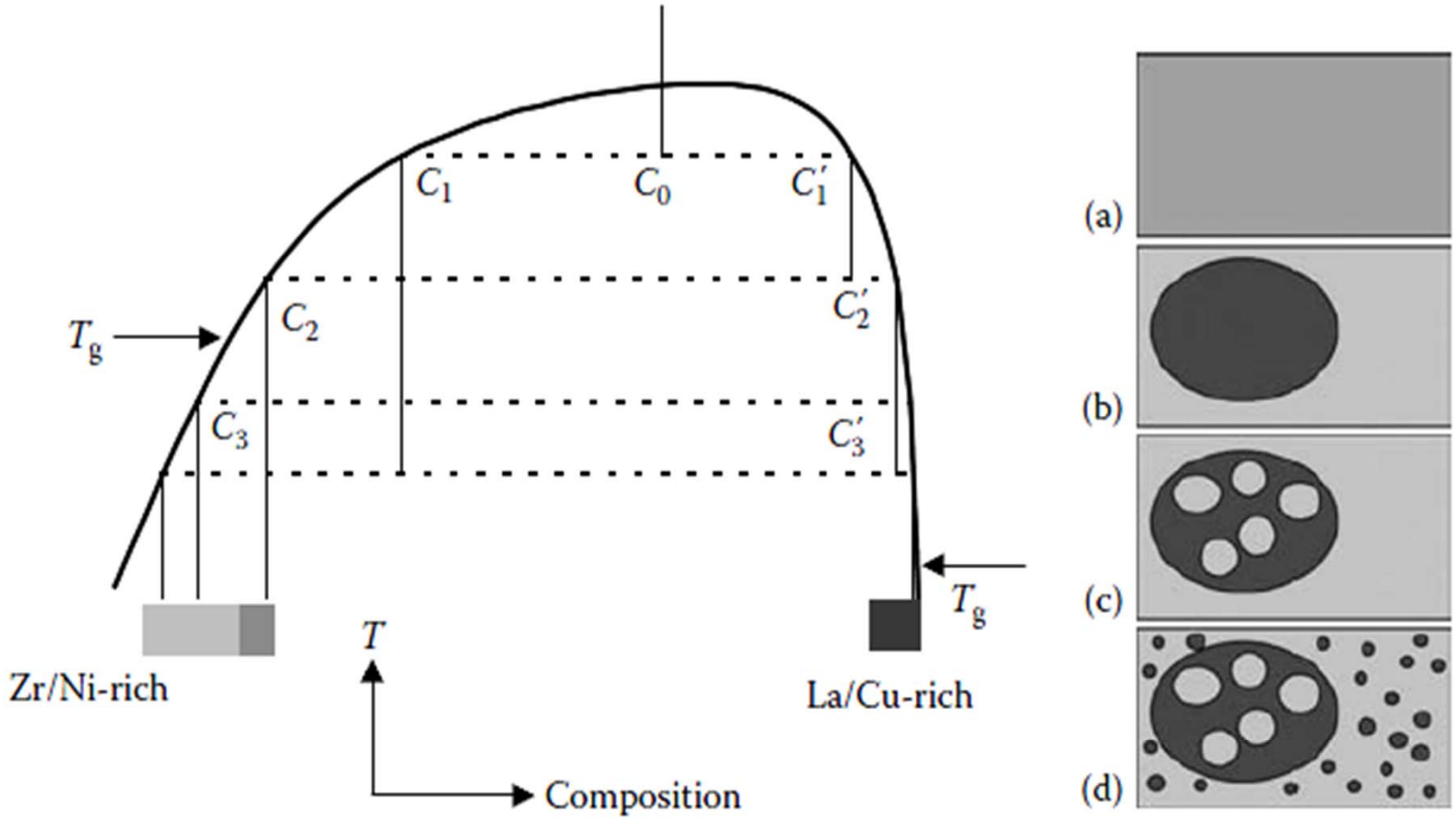

FIGURE 5.17
Schematic of the miscibility gap and the sequence of phase formation during cooling in the La–Zr–Al–Cu–Ni system. The positions of letters (a) to (d) in the diagram on the left correspond to the schematic microstructures (a) to (d) on the right. (Reprinted from Kündig, A.A. et al., *Acta Mater.*, 52, 2441, 2004. With permission.)

Shell/Yard region in phase separated structure

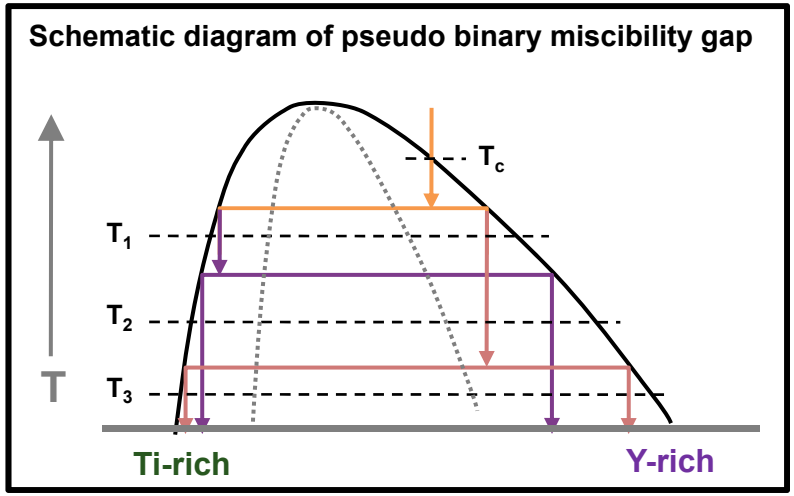

- Yard : Secondary phase-free region

  Shell : The layer enveloping primary phase by wetting

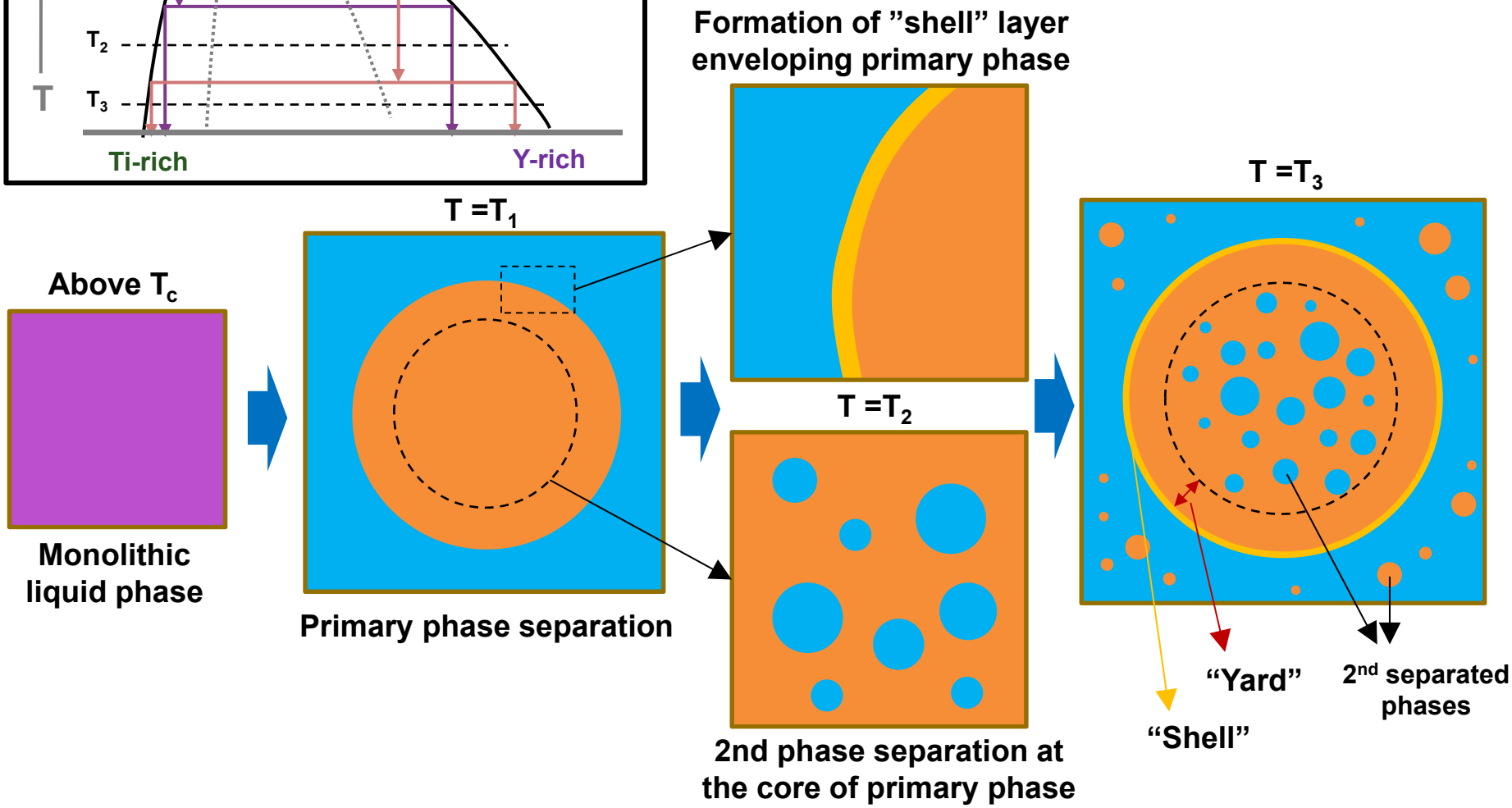

* Ti-Y-Al-Co system → $Ti_{24}Y_{18}La_{18}Al_{22}Co_{18}$ three different glassy phase

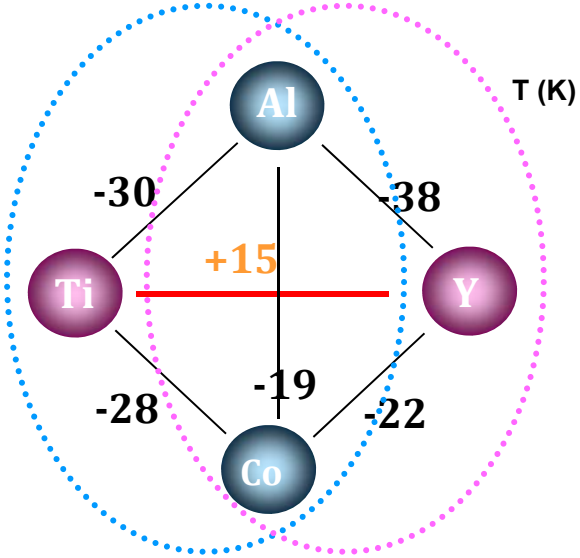

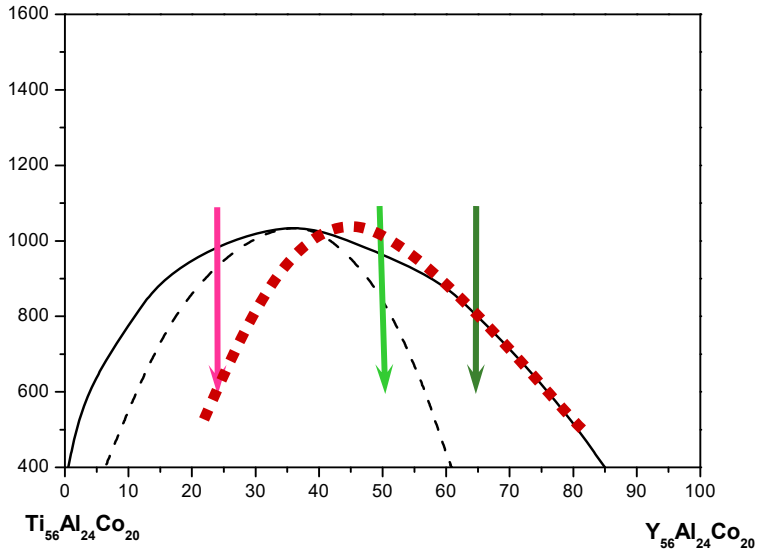

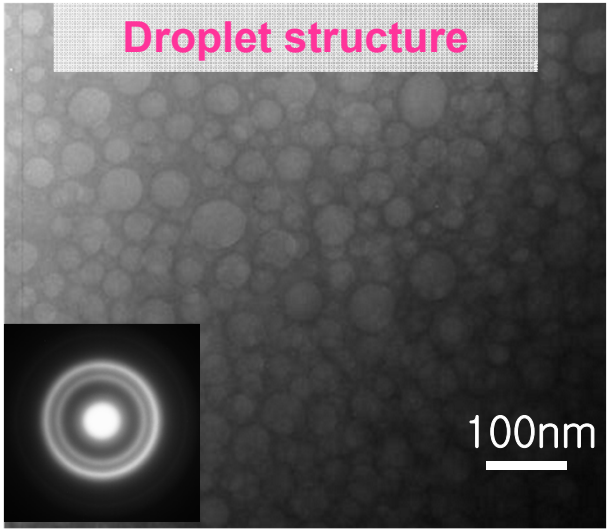

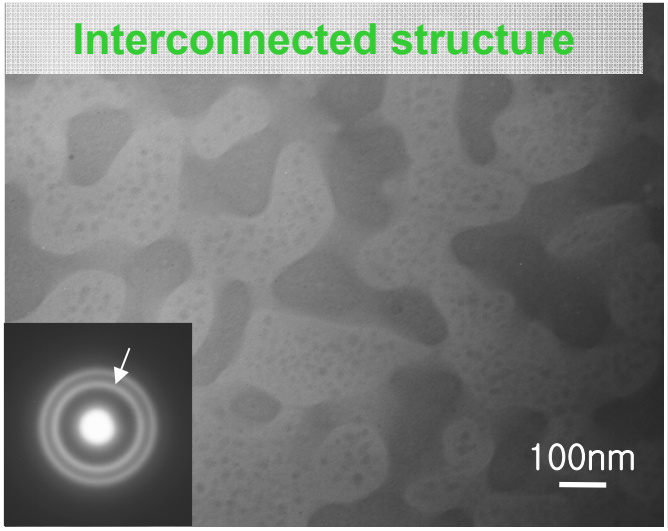

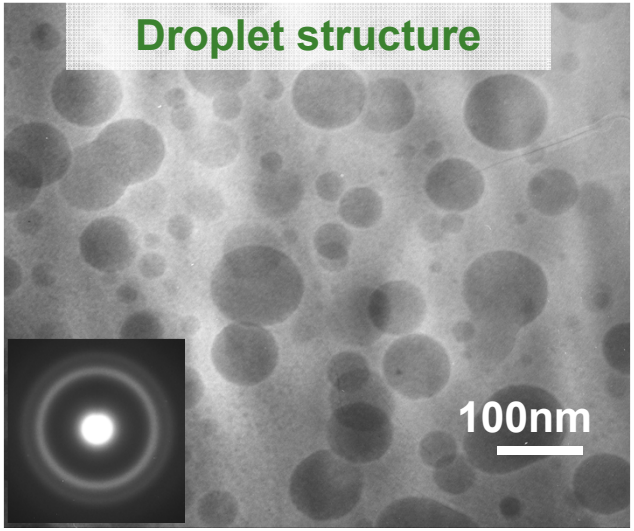

$(Y_{56}Al_{24}Co_{20})_{25}(Ti_{56}Al_{24}Co_{20})_{75}$ $(Y_{56}Al_{24}Co_{20})_{50}(Ti_{56}Al_{24}Co_{20})_{50}$ $(Y_{56}Al_{24}Co_{20})_{65}(Ti_{56}Al_{24}Co_{20})_{35}$

* Ti-Y-Al-Co system

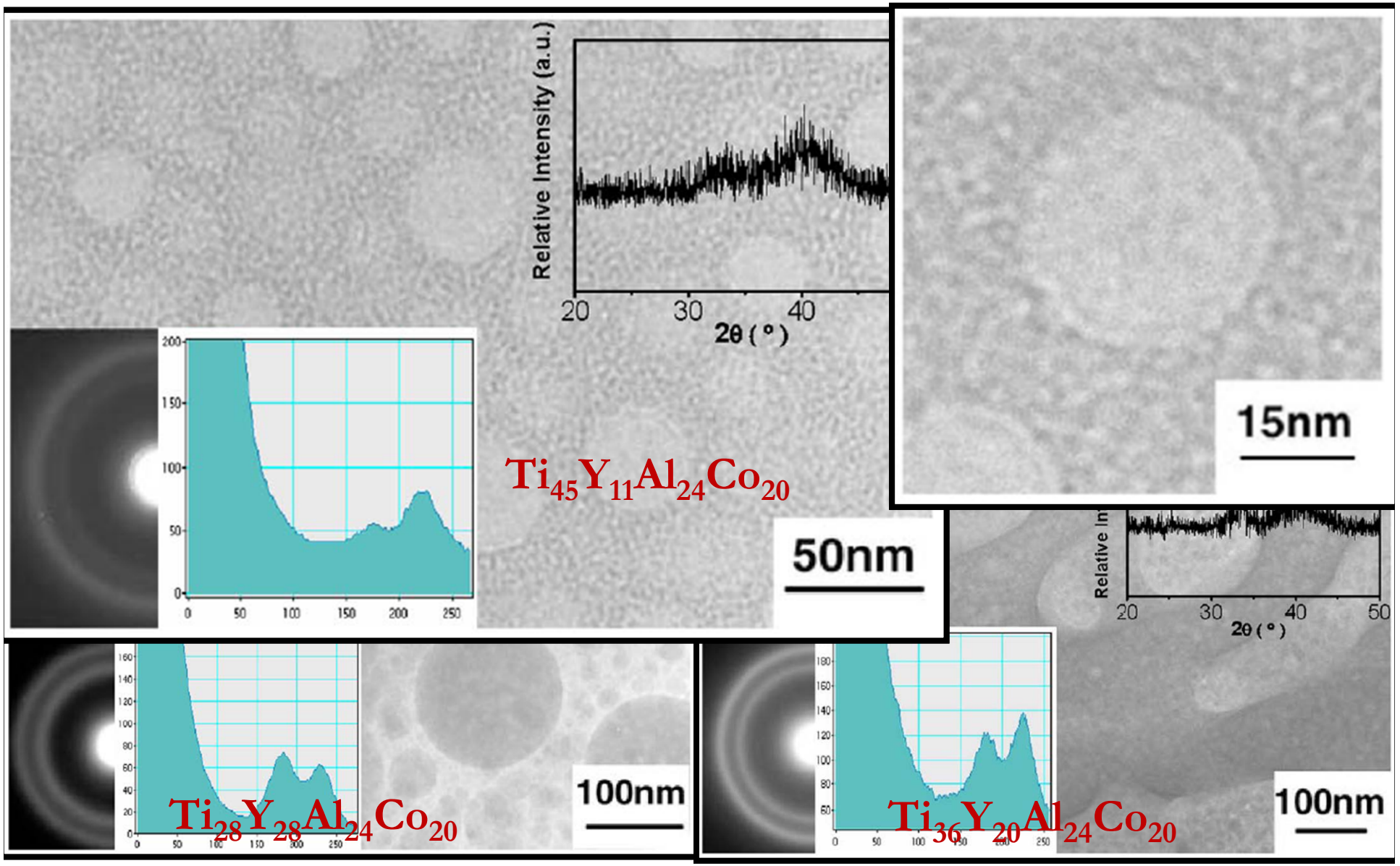

B.J.Park et al., *Appl. Phys. Lett.*. 85 (2004) 6353.
Phys. Rev. Lett., 96 (2006) 245503.

* Ni-Nb-Y system

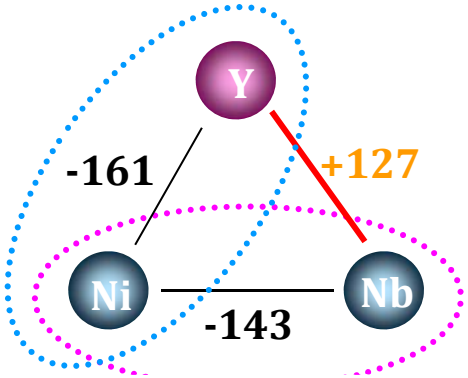

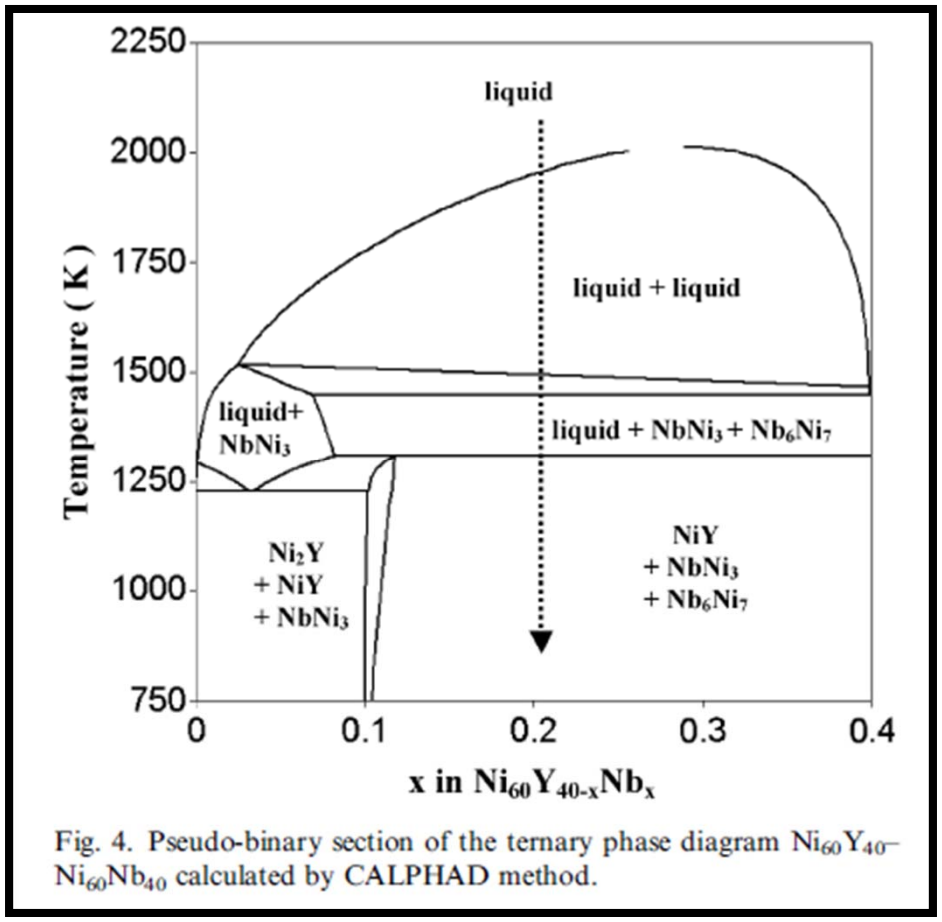

Fig. 4. Pseudo-binary section of the ternary phase diagram $Ni_{60}Y_{40}$–$Ni_{60}Nb_{40}$ calculated by CALPHAD method.

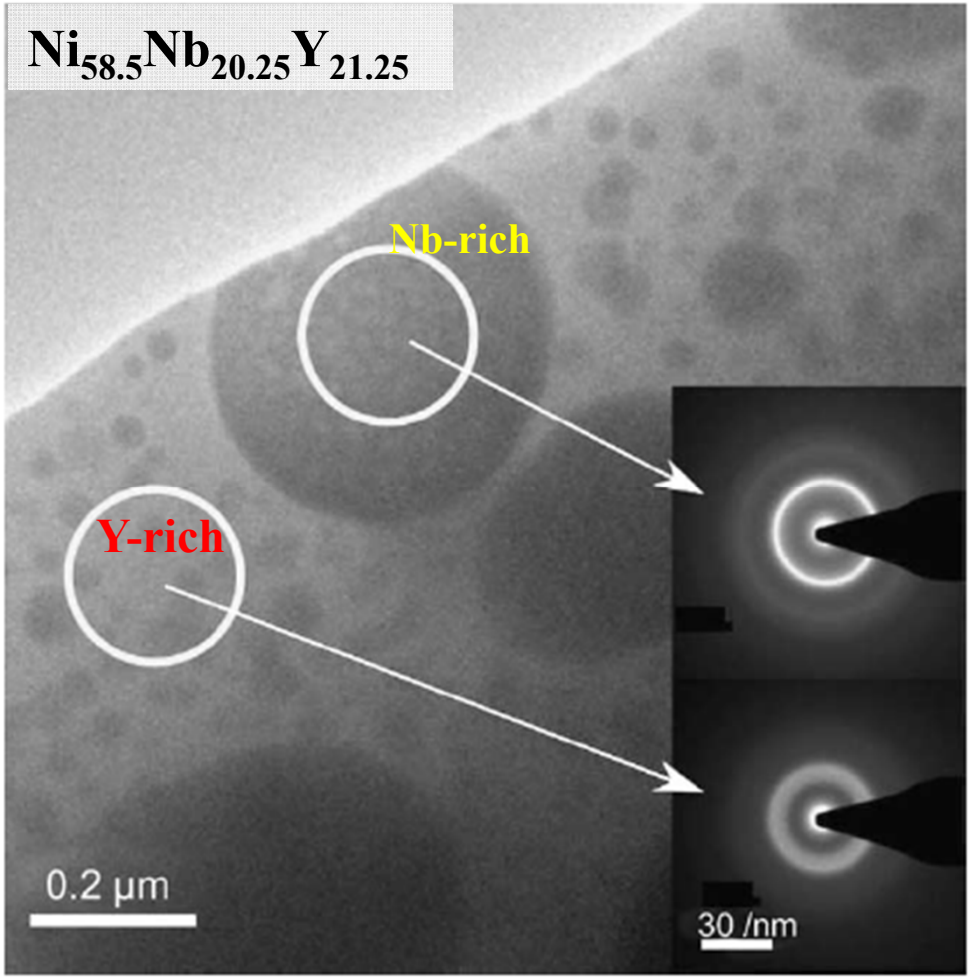

Mattern et al., *Scripta Mat.* 53 (2005) 271.
Mat. Sci. Eng. A, 449-451 (2007) 207.

Microstructure determining parameters of phase separation in metallic glasses

- ❖Composition
- ❖Glass-forming ability of the separated liquid
- ❖Critical temperature
- ❖Asymmetry of the spinodal curve / Decomposition range

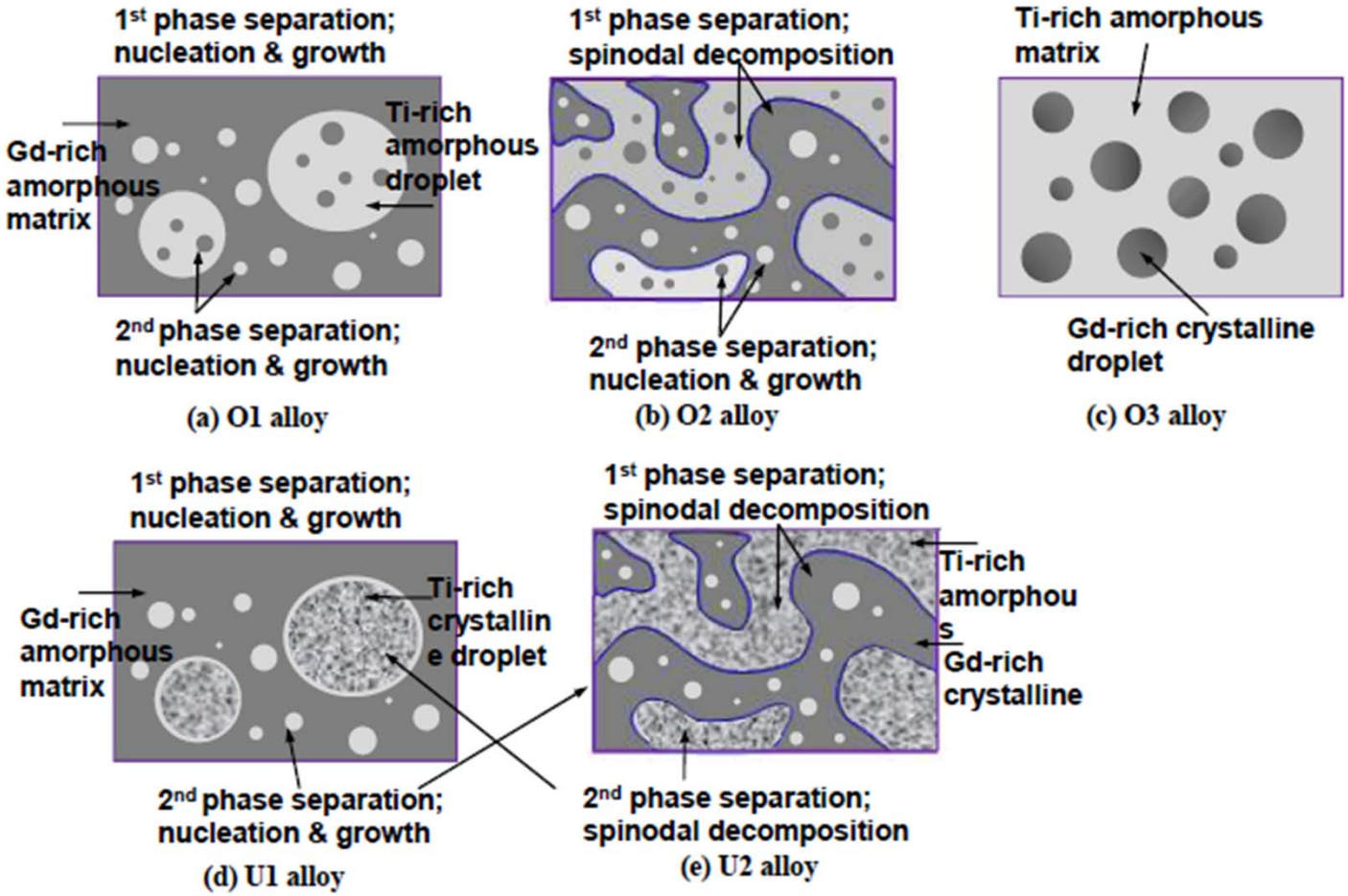

Thermodynamic calculation using CALPHAD

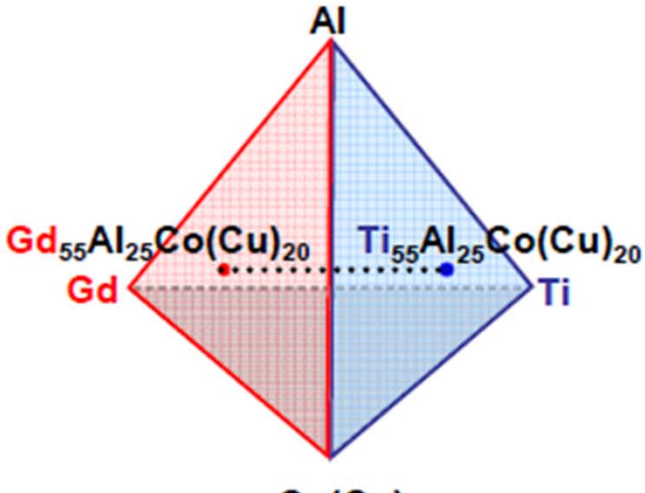

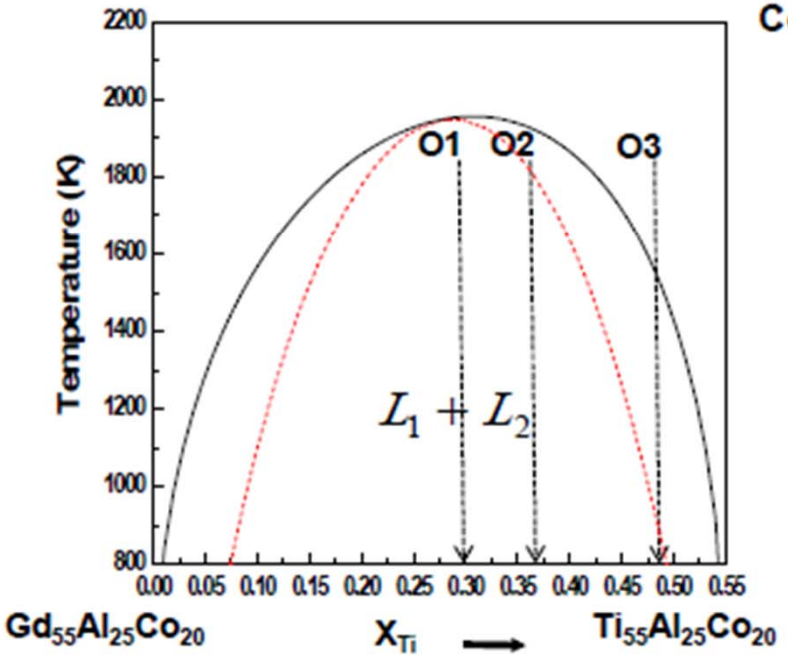

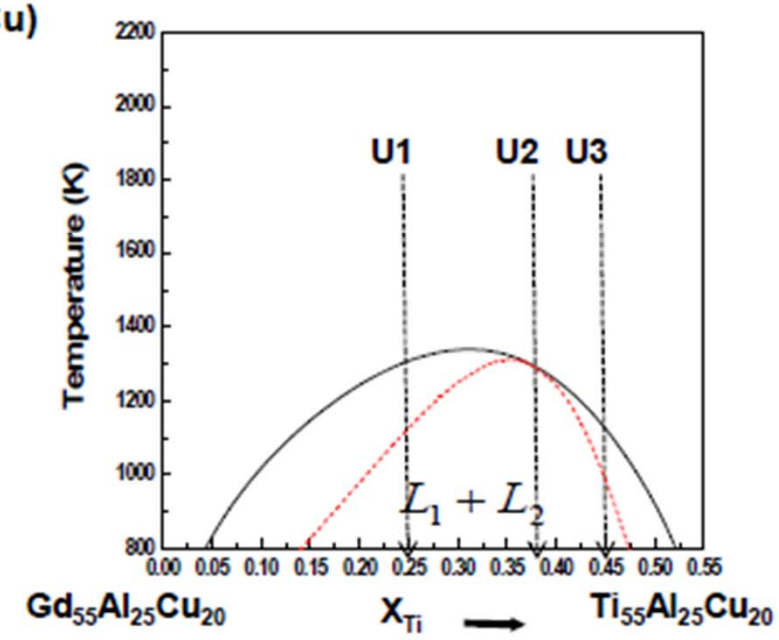

Microstructure evolution (GdTiAlCo)

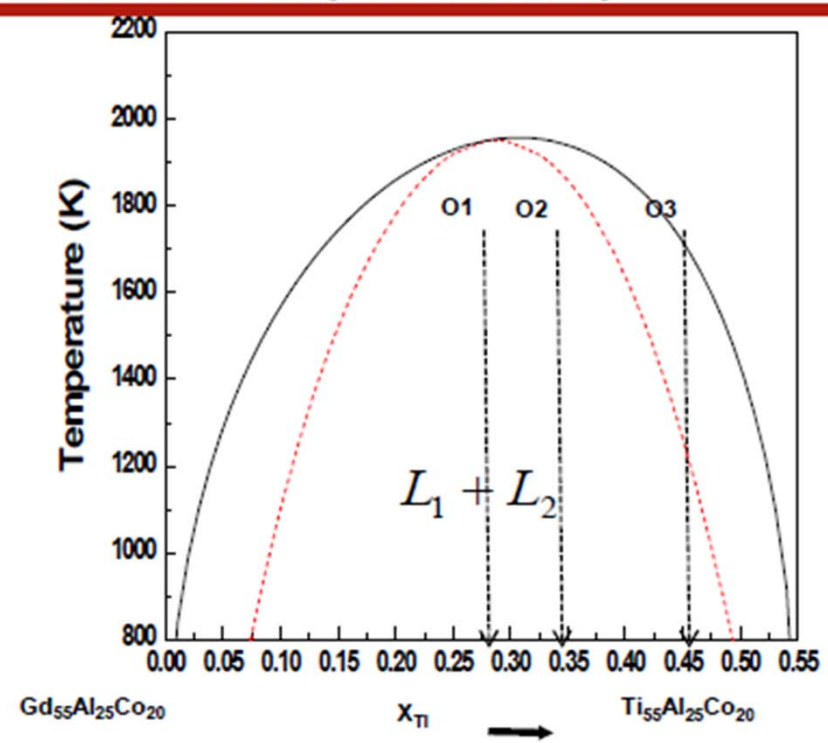

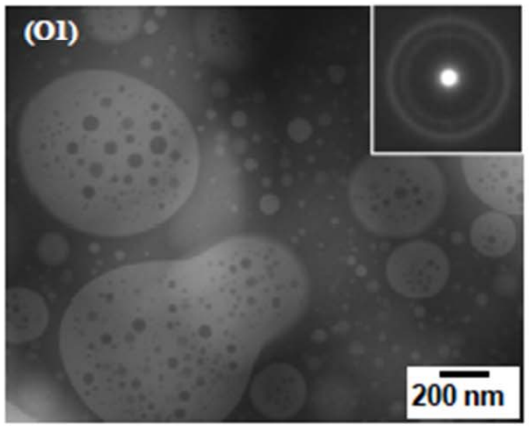

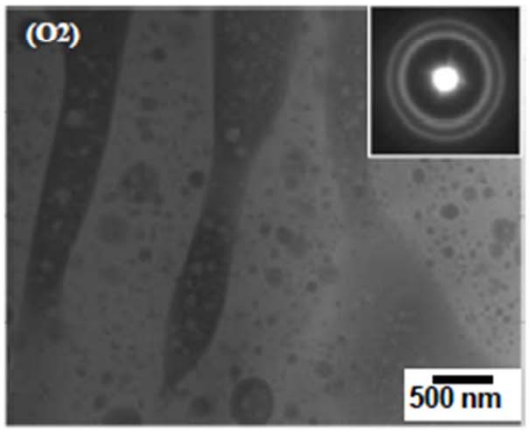

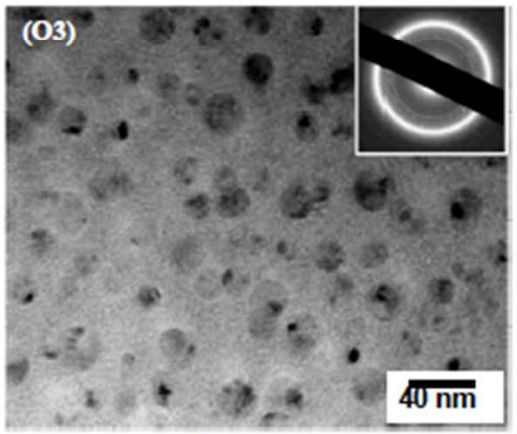

Chang et al., Acta Mater (2010)

Microstructure evolution (GdTiAlCu)

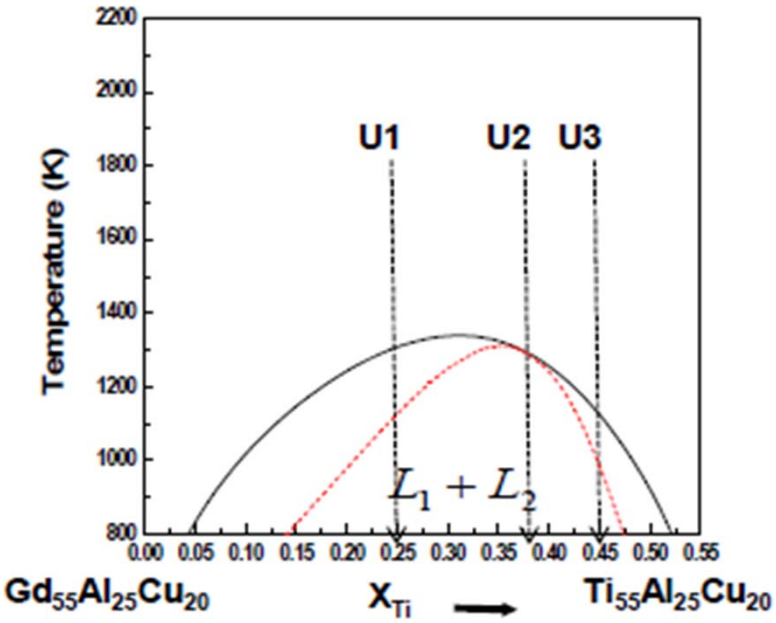

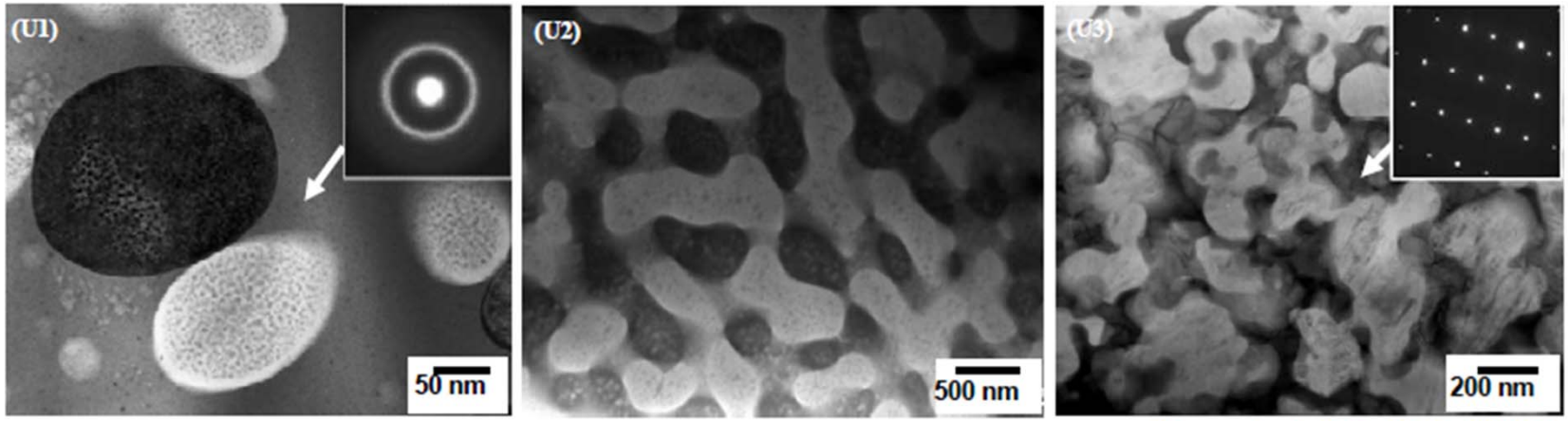

Chang et al., Acta Mater (2010)

Critical temperature

Spinodal critical point
$Gd_{25}Ti_{30}Al_{25}Co_{20}$ (at **1950 K**)

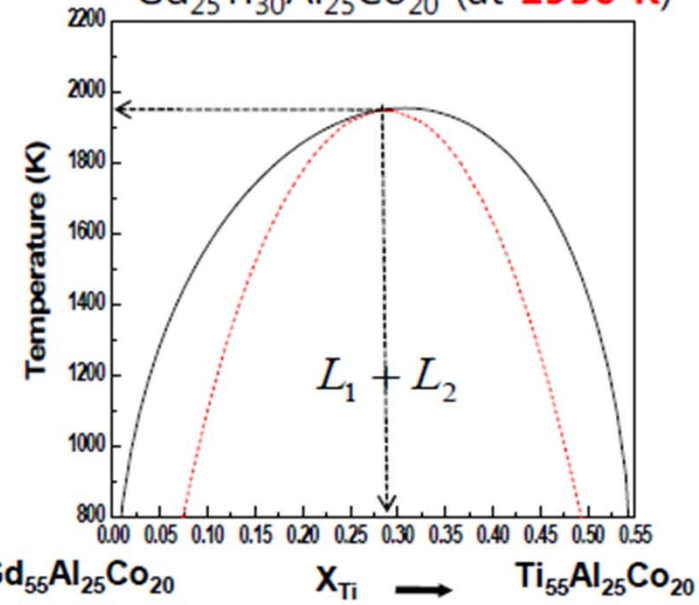

Spinodal critical point
$Gd_{18}Ti_{37}Al_{25}Cu_{20}$ (at **1300 K**)

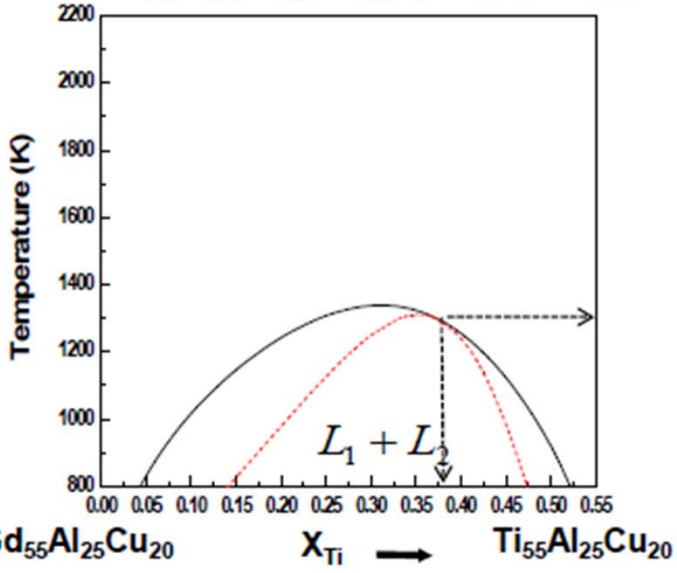

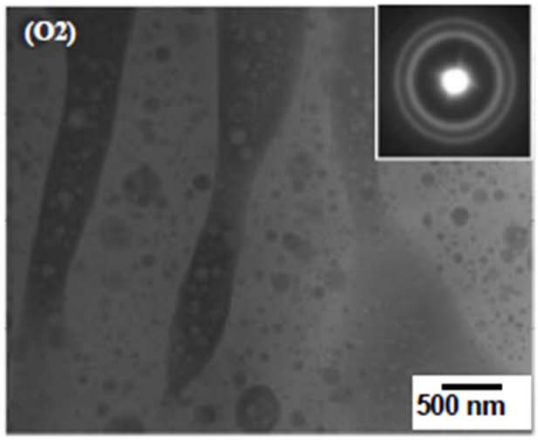

Scale of interconnected structure

←Several um

200~300 nm→

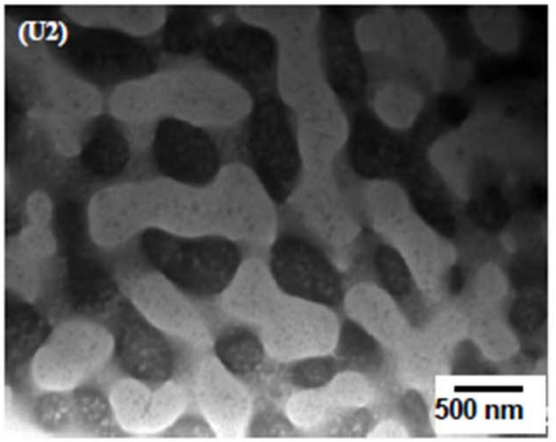

Asymmetry of spinodal curve / Decomposition range

❖ Symmetric spinodal curve / smaller decomposition range

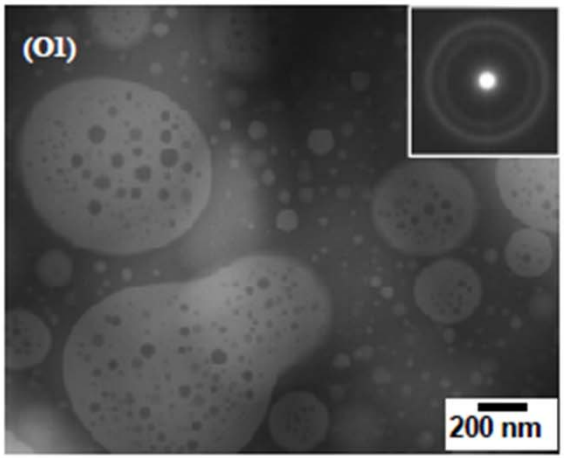

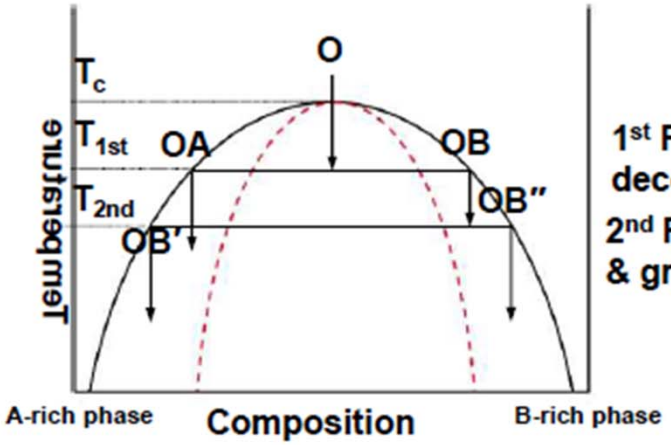

1st P.S.; spinodal decomposition

2nd P.S.; nucleation & growth

❖Asymmetric spinodal curve / larger decomposition range

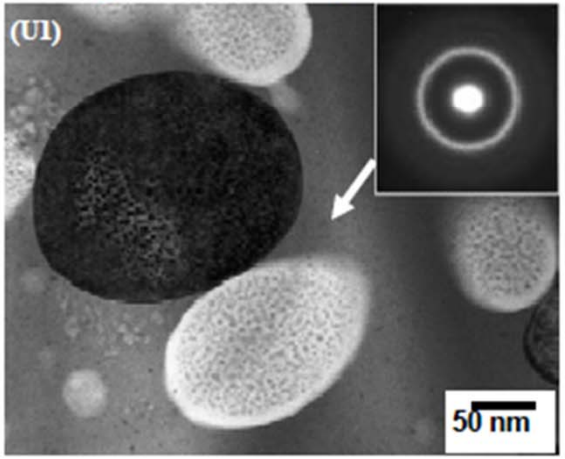

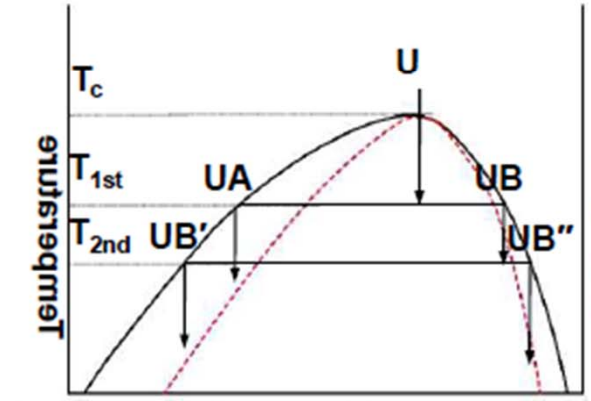

1st P.S.; spinodal decomposition

2nd P.S.; spinodal decomposition